eLife

Reviewed Preprint
v2 • August 13, 2025
Revised by authors

Reviewed Preprint
v1 • February 10, 2025

Cell Biology

Megakaryocytes assemble a three-dimensional cage of extracellular matrix that controls their maturation and anchoring to the vascular niche

Claire Masson, Cyril Scandola, Jean-Yves Rinckel, Fabienne Proamer, Emily Janus-Bell, Fareeha Batool, Naël Osmani, Jacky G Goetz, Léa Mallo, Nathalie Brouard, Catherine Léon, Alicia Bornert, Renaud Poincloux, Olivier Destaing, Alma Mansson, Hong Qian, Maxime Lehmann, Anita Eckly

Université de Strasbourg, INSERM, EFS Grand Est, BPPS UMR_S1255, FMTS, Strasbourg, France • Institut Pasteur, Université Paris Cité, Ultrastructural Bioimaging Unit, Paris, France • INSERM UMR_S1109, Tumor Biomechanics Lab, Université de Strasbourg, Fédération de Médecine Translationnelle de Strasbourg (FMTS), Strasbourg, France • Institut de Pharmacologie et de Biologie Structurale, Université de Toulouse, CNRS, UMR5089, Toulouse, France • Institute for Advanced Biosciences, Centre de Recherche Université Grenoble Alpes, Inserm U 1209, CNRS UMR 5309, Grenoble, France • Center for Hematology and Regenerative Medicine (HERM), Department of Medicine Hiddinge, Karolinska University Hospital, Karonlinska Institute, Stockholm, Sweden

eLife Assessment

In this revised version, the authors provide a thorough investigation of the interaction of megakaryocytes (MK) with their associated extracellular matrix (ECM) during maturation; they provide **compelling** evidence that the existence of a dense cage-like pericellular structure containing laminin γ1 and α4 and collagen IV is key to fixing the perisinusoidal localization of MK and preventing their premature intravasation. Adhesion of MK to this ECM cage is dependent on integrin beta1 and beta3 expressed by MK. This strong conclusion is based on the use of state-of-the art techniques such as the use of primary murine bone marrow MK cultures, mice lacking ECM receptors, namely integrin beta1 and beta3 null mice, as well as high-resolution 2D and 3D imaging. The study provides **valuable** insight into the role of cell-matrix interactions in MK maturation and provides an interesting model with practical implications for the fields of hemostasis and thrombosis

https://doi.org/10.7554/eLife.104963.2.sa3

Abstract

Megakaryocytes, the progenitor cells of blood platelets, play a crucial role in hemostasis by residing in the bone marrow and ensuring continuous platelet production. Unlike other hematopoietic cells, megakaryocytes do not enter the blood circulation intact. They remain anchored within the bone marrow while extending cytoplasmic protrusions called proplatelets through the sinusoidal endothelial barrier. These proplatelets subsequently fragment into functional platelets. This unique process of intravasation facilitates efficient

platelet production while maintaining the megakaryocyte cell body within the bone marrow niche, thus preventing potential thrombotic complications. How the extracellular matrix (ECM) influences the delicate balance between megakaryocyte retention and proplatelet extension remains largely unknown. Here, we investigate the spatial organization and functional role of ECM components in the megakaryocyte vascular niche. Our findings reveal that laminin and collagen IV form three-dimensional (3D) ECM cages encompassing megakaryocytes and anchor them to the sinusoidal basement membrane. Gene deletion shows the existence of laminin α4 in the ECM cage that is necessary to maintain megakaryocyte-sinusoid interactions. Notably, megakaryocytes actively contribute to the ECM cage assembly; β1/β3 integrin knockout weakens these structures, increasing intravasation and entire megakaryocyte entry into circulation. The retention of megakaryocytes by these 3D ECM cages depends on dynamic remodeling processes. Inhibition of ECM proteolysis results in denser cage formation, increasing the frequence of immature megakaryocytes with impaired demarcation membrane system (DMS) development. Thus, the ECM cage represents a novel concept of an active and dynamic 3D microenvironment that is continuously remodeled and essential for maintaining megakaryocyte perivascular positioning. This specific microarchitecture guides megakaryocyte maturation and intravasation, underscoring the critical role of ECM microarchitecture and dynamics in megakaryocyte function.

Key Points

1. Megakaryocytes form a three-dimensional (3D) cage composed of laminin and collagen IV connected to the basement membrane surrounding them. This microarchitecture stabilizes megakaryocytes within their vascular niche.
2. β1/β3 integrins and MMP are key ECM cage regulators that assist megakaryocyte maturation and intravasation at the bone marrow-blood interface.

Introduction

Megakaryocytes, the precursors of blood platelets, differentiate from hematopoietic stem cells and mature in a complex bone marrow microenvironment. Megakaryocytes are large, highly polyploid cells that contain a complex invaginated network of membranes, known as the demarcation membrane system (DMS), which serves as a membrane reservoir for platelet production. In contrast to other hematopoietic cells, megakaryocytes exhibit a unique platelet production process. They do not enter the bloodstream intact. Instead, they remain anchored in the bone marrow and extend cytoplasmic protrusions called proplatelets through the sinusoidal endothelial barrier. These protrusions protrude into the lumen of bone marrow sinusoids, where they undergo fragmentation to release individual platelets into the circulation. This distinctive mechanism allows for the efficient production and release of platelets while maintaining the megakaryocyte cell body within the bone marrow microenvironment, thus reducing the risk of thrombotic complications (Boscher et al., 2020; Stone et al., 2022). The remaining cell body, composed of a nucleus surrounded by a thin rim of cytoplasm, is ultimately phagocytosed in the stroma (Radley & Haller, 1983).

Megakaryocytes are strategically located at the interface between the bone marrow and the blood circulation, specifically at the parasinusoidal region (Lichtman et al., 1978; Stegner et al., 2017). Intravasation, the coordinated passage of megakaryocyte fragments through the sinusoidal barrier, requires an original, complex, and dynamic adaptation of megakaryocytes to highly different microenvironments, both mechanically and biologically. They are positioned next

to the endothelial lining and its underlying basement membrane, in equilibrium between the constrained 3D environment of the bone marrow and the fluid environment of the blood. In this context, they are in contact with two types of ECM organization: basement membrane and interstitial ECM.

Megakaryocytes actively influence their structural microenvironment through several ECM remodeling mechanisms, including the endocytosis of plasma proteins like fibrinogen, and the synthesis and release of extracellular matrix (ECM) components such as fibronectin laminin, and type IV collagen (Abbonante et al., 2017; Handagama et al., 1987; Malara et al., 2014). Additionally, they produce ECM-modifying proteins, including matrix metalloproteinases (MMPs), tissue inhibitors of metalloproteinases (TIMPs), and lysyl oxidase (LOX), which facilitate the continuous renewal and regulation of the matrix (Eliades et al., 2011; Malara et al., 2018; Villeneuve et al., 2009). Furthermore, we have recently discovered that megakaryocytes could remodel the substrate-bound fibronectin matrix into basal fibrillar structures surrounding the cells. The extent of fibrillogenesis depended on the stiffness of the substrate, and relied on both β1 and β3 integrins (Guinard et al., 2023). This intricate interplay between megakaryocytes and their surrounding ECM remodeling demonstrates the dynamic nature of the vascular niche and highlights its critical role in platelet production.

The ECM surrounding megakaryocytes plays a crucial role in their development and function. Numerous studies have identified essential components of this matrix, including collagen IV, fibronectin, fibrinogen, and laminin (Larson & Watson, 2006; Malara et al., 2014; Semeniak et al., 2016; Susek et al., 2018). The presence and function of collagen I fibers remain a subject of ongoing debate, with some researchers proposing that they guide megakaryocyte proplatelets toward sinusoids (Oprescu et al., 2022). *In vitro* studies have shown that while collagen I may inhibit proplatelet formation, other ECM components, like collagen IV, fibrinogen, and fibronectin, can facilitate this process (Balduini et al., 2008; Malara et al., 2014; Sabri et al., 2004). The diverse and sometimes contradictory roles of these ECM components in megakaryocyte behavior underscore the complexity of this research area and highlight the need for further investigation, particularly *in vivo*.

The present study provides new insight into the spatial organization of the ECM that envelops megakaryocytes, elucidating its specific architecture and molecular mechanisms governing its dynamics and function. We performed advanced 2D and 3D analyses of mouse bone marrow and identified a novel ECM cage containing laminin chains Y1 and α4, and collagen IV that anchored megakaryocytes to the sinusoidal basement membrane. Deleting laminin α4 impairs the connections between megakaryocytes and sinusoids. Megakaryocytes act actively in forming and maintaining this ECM cage, relying on their integrins β1 and β3. Indeed, deleting these integrins causes significant impairment of the cage's integrity, resulting in increased intravasation of megakaryocytes and an unexpected release of intact megakaryocytes into the bloodstream. Moreover, *in vivo*, matrix metalloproteinases (MMPs) inhibition reveals that dynamic ECM remodeling is crucial for maintaining the cage structure and supporting megakaryocyte development. In conclusion, our study unveils a 3D ECM cage that physically stabilizes megakaryocytes within their vascular niche. This structure facilitates the physiological regulation of megakaryocyte maturation and intravasation at the bone marrow-bloodstream interface.

Results

Laminin and collagen IV create a 3D cage around sinusoid-associated megakaryocytes

The organization of the ECM around megakaryocytes in the vascular niche is not well understood due to challenges in *in vivo* observation. To investigate this, we utilized immunofluorescence (IF) microscopy on ultrathin bone marrow cryosections (250 nm thickness). This approach offers superior axial resolution compared to traditional confocal microscopy, enabling high-resolution localization of ECM components. Megakaryocytes were visualized using antibodies against GPIbβ, while sinusoids were identified with antibodies against FABP4 (**Figure 1A**). Our findings revealed that laminin Y1 chains and collagen IV delineated the basement membrane underlying the endothelium of sinusoids and the outer contour of mature megakaryocytes (**Figure 1A**, **Suppl. Figure 1Aa**). Adjacent cells exhibited granular staining for laminin Y1 and collagen IV, which may indicate a potential contribution to the ECM constitution (arrow in **Suppl. Figure 1Ag-h**). Fibronectin was detected in the basement membrane and around megakaryocytes, while fibrinogen was more widespread, associated with the basement membrane, the megakaryocyte surface, and intracellular granules (**Suppl. Figure 1Ab-c**). Von Willebrand factor (VWF) signal was restricted to the alpha granules of megakaryocytes (**Suppl. Figure 1Ad**). We observed no detectable signals for type I and III collagen around megakaryocytes or sinusoids despite using antibodies validated on positive controls (**Suppl. Figure 1Ae-f**, **Suppl. Figure 1B-C**).

Having established the expression of laminin Y1, collagen IV, fibronectin, and fibrinogen in the direct megakaryocyte microenvironment, their spatial organization was next investigated using 3D imaging of whole-mount bone marrow preparations (**Figure 1B**). Analysis of maximum Z-stack projections revealed that laminin Y1 and collagen IV formed a reticular 3D ECM cage completely enveloping megakaryocytes and extending radially from the sinusoidal basement membrane (**Figure 1B-C**). With this approach, the basement membrane-ECM cage connections were clearly visible when examining the full z-stack series. Examples are shown in movies 1 and 2 and in **Suppl. Figures 1D-E**. Quantification showed that almost all megakaryocytes near sinusoids (sMK, 92.8 ± 3.3 %) have a laminin cage, compared to only 11.4 ± 4.8 % of megakaryocytes in the parenchyma (pMK) (**Suppl. Figure 1F-G**). Parenchymal megakaryocytes (pMK), which represented only 18 ± 1.3 % of all megakaryocyte population (**Suppl. Figure 1H**), were instead surrounded by a a sparse thin network of laminin Y1 (**Suppl. Figure 1F**). Althought we cannot exclude that ECM cage can be form on its own, our data suggests that ECM cage assembly may require interactions between megakaryocytes and the sinusoidal basement membrane. Parenchymal megakaryocytes (pMK), which represented only 18 ± 1.3 % of all megakaryocyte population (**Suppl. Figure 1H**), were instead surrounded by a a sparse thin network of laminin Y1 (**Suppl. Figure 1F**). The ECM cage was present at all stages of megakaryocyte maturation, including megakaryocytes with proplatelet extension (**Suppl. Figures 1I-J**). Remarkably, after mechanical dissociation and size exclusion, nearly half of the megakaryocytes successfully retained their cages (53.4 ± 5.6 %, 329 megakaryocytes counted from 3 mice), indicating strong physical attachments between both components (**Figure 1D**). While fibronectin and fibrinogen are present around megakaryocytes and at the vessel-cell interface, they do not form a reticular ECM cage. Furthermore, no connection was found between fibronectin and fibrinogen deposition with the sinusoid basement membrane, in contrast to the findings for laminin and collagen IV (**Suppl. Figure 1K**). These observations demonstrate that megakaryocytes establish precise and tight interactions with an ECM cage made of laminin Y1 and collagen IV in a spatially confined microenvironment at the sinusoidal basement membrane.

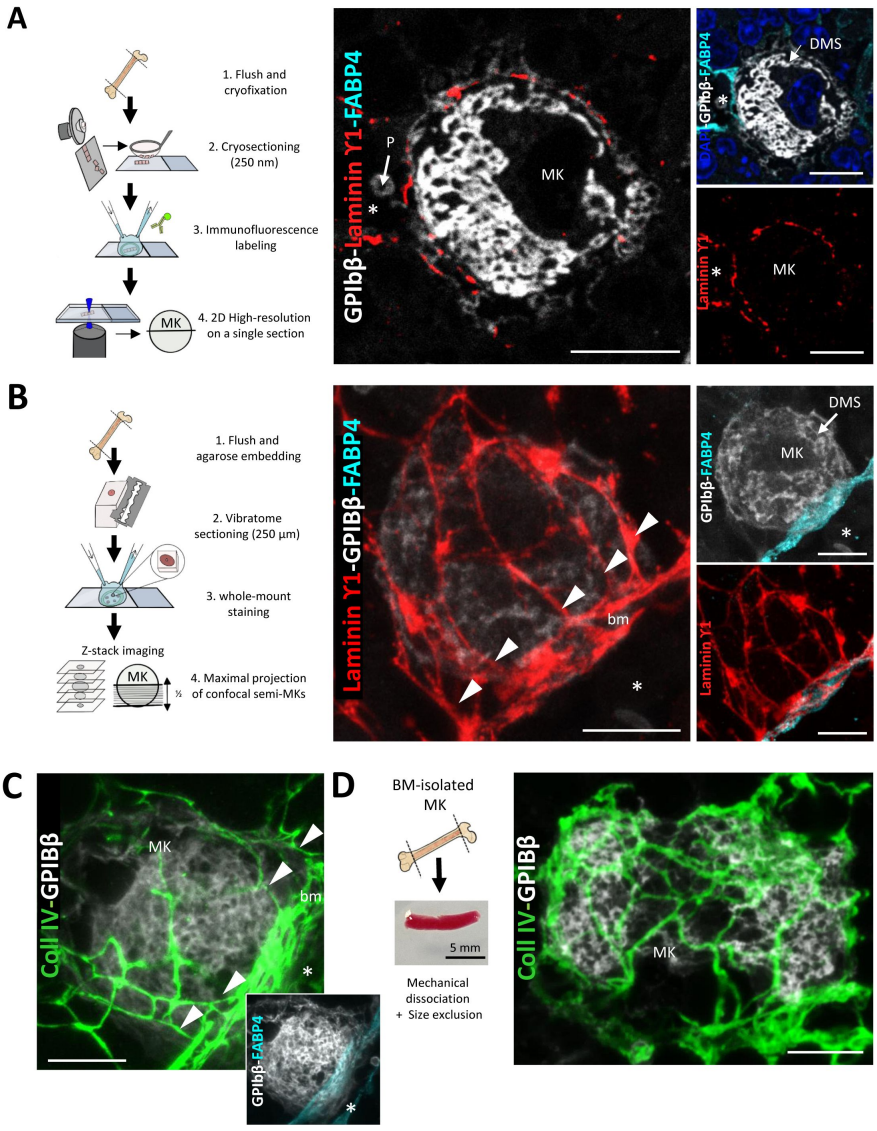

Figure 1

LaminiY1 and collagen IV form 3D cages of ECM for megakaryocytes, directly connected to the sinusoidal basement membrane

(A) Left panel. Schematic representation of the experimental workflow for 2D imaging of immunostained bone marrow cryosections from WT mice. Confocal imaging is performed on single ultrathin sections with an axial resolution of 250 µm. Right panel. Representative 2D images of a sinusoid-associated megakaryocyte immunostained for laminin Y1 (red), GPIbβ (white) and FABP4 (cyan). Cell nuclei are visualized with DAPI (blue) (from one out of three independent IF experiments).
(B) Left panel. Schematic representation of the experimental workflow for 3D analysis of whole-mount bone marrow preparations from WT mice. A stack of confocal images covering half the depth of the megakaryocyte is acquired and then z-projected to create a maximum projection image. Right panel. Representative maximal projection images of sinusoid-associated megakaryocyte immunostained for laminin Y1 (red), GPIbβ (white) and FABP4 (cyan) (from one out of three independent IF experiments).
(C) Representative maximal projection images of sinusoid-associated megakaryocyte immunostained for collagen IV (green) and GPIbβ (white). The inset image shows the FABP4 (cyan) and megakaryocyte (white) immunostaining.
(D) Bone marrow-isolated megakaryocyte maintaining an ECM cage. Left panel. Schematic of the experimental procedure used to isolate mouse bone marrow megakaryocytes. Right panel. Maximal projection 3D images showing the persistence of the ECM cage (collagen IV in green) around a freshly isolated megakaryocyte (GPIbβ in white).
*, sinusoid lumen ; arrowheads, basement membrane-cage connections; BM, bone marrow; bm, basement membrane ; MK, megakaryocyte; Bars, 10 µm.

Reduced 3D laminin cage and vessel-associated megakaryocytes in Lamα4$^{-/-}$ mouse bone marrow

Among the γ1 chain-bearing laminin isoforms, laminin α4 was abundantly found in bone marrow sinusoid basement membrane (Susek et al., 2018). To explore the direct influence of ECM organization on platelets and megakaryocytes, we utilized laminin α4-deficient mice (Lamα4$^{-/-}$). These mice exhibit mild thrombocytopenia, with platelet counts approximately 20% lower than wild-type (WT) mice (Cai et al., 2022). Their platelets maintain a normal ultrastructure and functions, as shown by flow cytometry and EM analysis (**Suppl. Figures 2A-C**). Bone marrow from Lamα4$^{-/-}$ mice showed a normal number of mature megakaryocytes with characteristic ultrastructural features (**Figure 2C** and **Suppl. Figure 2D**). Analysis of bone marrow explants further demonstrated that these megakaryocytes could extend proplatelets, indicating preserved fundamental function (**Suppl. Figures 2 E-F**).

We next examined the ECM cage using an antibody against laminin γ1. In Lamα4$^{-/-}$ mice, laminin γ1 deposition around megakaryocytes and in the sinusoid basement membrane decreased by 1.7- and 2.6-fold compared to controls, indicating a disruption of the laminin cage (**Figures 2A-B**, upper panels). However, collagen IV organization remained unaltered around the megakaryocytes in these mice (**Figure 2A-B**, lower panels), showing that laminin α4 is not necessary for collagen IV cage formation. We also analyzed megakaryocyte localization in the bone marrow of Lamα4$^{-/-}$ mice (**Figure 2C**). The total megakaryocyte density was similar to that of control mice (**Figure 2D**), but we observed more parenchymal MK with a 1.5-fold reduction in the number of megakaryocytes near sinusoids (**Figure 2E**). These observations highlights the role of the laminin α4 cage in maintaining optimal positioning of megakaryocytes near sinusoids.

Integrins maintain the structural properties of the ECM cages

Integrins play a crucial role in ECM remodeling. Megakaryocytes express β1 and β3 integrins as main ECM receptors (Yang et al., 2022). To elucidate the molecular mechanisms governing the intricate interactions between megakaryocytes and the ECM cage, we investigate the subcellular localization of integrins on immunostained ultrathin bone marrow cryosections. Using conformation-independent antibodies, we showed the presence of β1 subunit at on the plasma membrane and on the DMS (**Figure 3A**). Similar findings were obtained for total β3 integrins (**Suppl. Figure 3A**). In contrast, the activated form of β1 integrin was expressed only at interaction sites with laminin γ1 and collagen IV, suggesting that activated β1 integrins mediate megakaryocyte interactions with the ECM cage (**Figure 3B**). Activated β3 integrin involvement remains to be determined, as no specific signal was detected when testing two different antibodies (JonA-PE, Pac 1).

To test if integrin-mediated signaling plays a role in the structural assembly of the ECM cage, a transgenic mouse model lacking β1 and β3 integrins in the megakaryocyte lineage was used (*Itgb1*$^{-/-}$*/Itgb3*$^{-/-}$*)* (**Figure 3C**). *Itgb1*$^{-/-}$*/Itgb3*$^{-/-}$ mice were generated crossing the two single loxP-flanked lines (β1$^{fl/fl}$ and β3$^{fl/fl}$ mice) with *Pf4-Cre* mice (expressing the Cre recombinase under the control of the *Pf4* promoter). Our analysis revealed a 2.6-fold reduction in laminin γ1 deposition on the megakaryocyte surface in *Itgb1*$^{-/-}$*/Itgb3*$^{-/-}$ mice compared to *Pf4-Cre* control mice. Furthermore, intensity profiles demonstrated that laminin γ1 forms a less dense network around the megakaryocytes in the double knockout mice, with significantly increased mesh sizes (10.6 ± 1.3 µm vs 6.3 ± 0.6 µm, respectively) (**Figure 3D**). Notably, this lower ECM density surrounding megakaryocytes in *Itgb1*$^{-/-}$*/Itgb3*$^{-/-}$ mice is not linked to increased matrix degradation or reduced laminin synthesis (**Suppl. Figures 3B-C**). As expected, the laminin γ1 network at the basement membrane remained unaffected in these mice, as the integrin deletion is restricted to megakaryocytes (**Suppl. Figures 3E-F**).

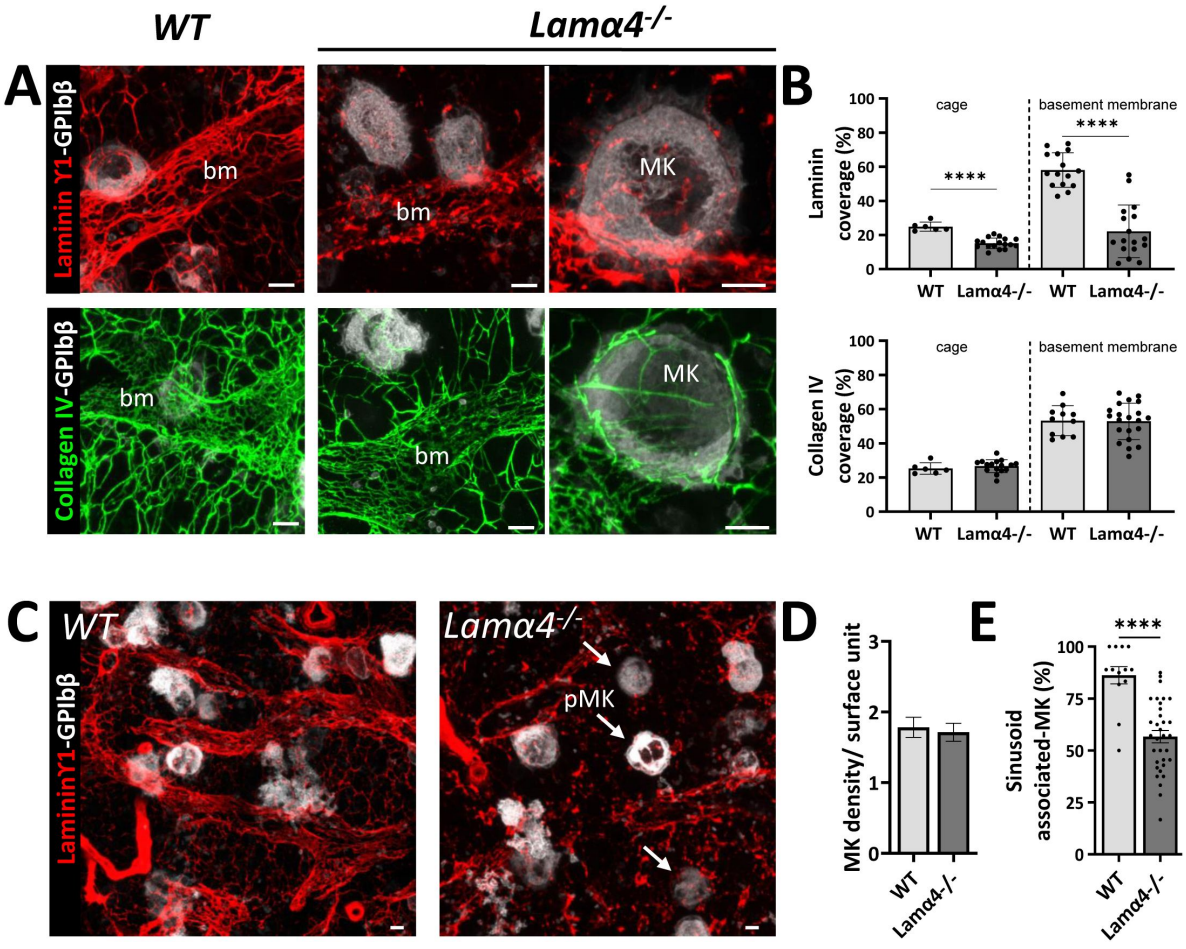

Figure 2

Reduced laminin Y1 cage and megakaryocyte-sinusoid interactions in *Lamα4*$^{-/-}$ mouse bone marrow.

(A-B) Depletion of laminin α4 leads to a reduction in the laminin Y1 deposition, but not in collagen IV, in the cage around megakaryocytes and in the sinusoid basement membrane.

A. Representative maximal projection images showing the immunostaining of laminin γ1 (red) or collagen IV (green) in the *Lamα4*$^{-/-}$ compared to control mice. Two magnifications are shown for *Lamα4*$^{-/-}$ mouse.

B. Quantification of laminin γ1 and collagen IV surface coverage per megakaryocyte and per basement membrane surface (laminin: 6<cage<17 and 15<bm<17; collagen IV: 6<cage<16 and 11<bm<21 expressed as a percentage, ****P>0.001 unpaired t-Test).

(C-E) Depletion of laminin α4 leads to a decrease in the sinusoid-associated megakaryocytes.

C. Representative maximal projections showing the immunostaining of laminin γ1 (red) and megakaryocytes (GPIbβ in white) in the bone marrow of *Lamα4*$^{-/-}$ and control mice.

D. Quantification of the total number of megakaryocytes per surface unit (s.u., 12,945 μm^2, n=3 for each genotype, 87<n<92, P=0.9228, ns, Mann-Whitney test).

E. Quantification of the sinusoid-associated megakaryocytes (n=3, ****P>0.001 unpaired t-Test) in control (grey) and *Lamα4*$^{-/-}$ (dark) mice. Arrows point to megakaryocytes which are not associated with sinusoids (pMK).

bm, basement membrane; MK, megakaryocyte; pMK, MK in the parenchyma; Bar, 10 μm.

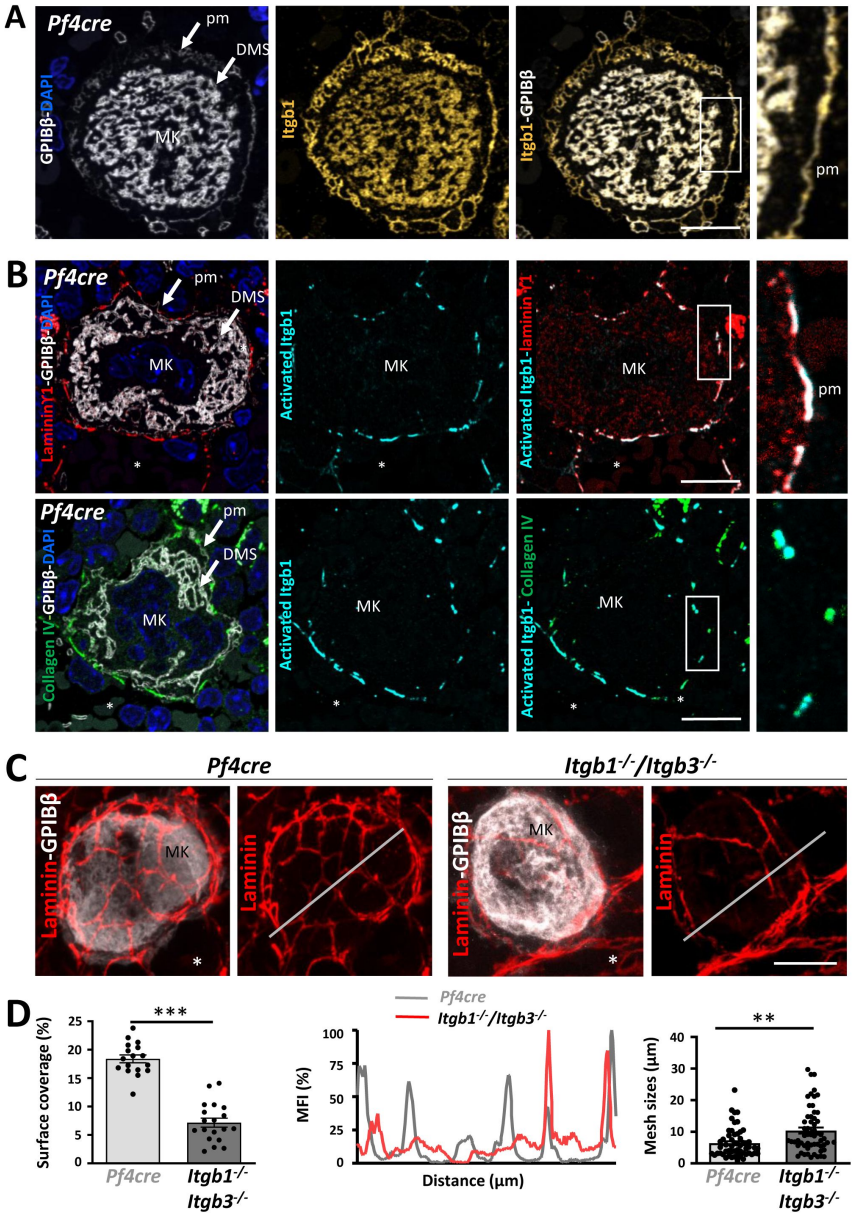

Figure 3

Integrin-mediated control of the 3D ECM cage around megakaryocytes

(A) Representative 2D images of *Pf4cre* bone marrow cryosections (250 nm) showing a sinusoid-associated megakaryocyte immunostained for β1 integrin (MAB1997 in yellow). Right: the boxed area is shown at a higher magnification.
(B) Activated β1 integrins form functional adhesion structures around megakaryocyte surfaces. Representative 2D images of *Pf4cre* bone marrow cryosections showing laminin (red, upper panels) or collagen IV (green, lower panels) staining around a sinusoid-associated megakaryocyte immunostained for activated β1 integrin (9EG7 in cyan) and GPIbβ (white). Right: Magnification of the boxed area showing co-localization of the ECM proteins and activated β1 integrin.
(C) Depletion of β1 and β3 integrins leads to a reduction in the laminin deposition on the surface of megakaryocytes. Representative 3D images showing a decrease in laminin deposition (red) on *Itgb1*$^{-/-}$/*Itgb3*$^{-/-}$ megakaryocytes compared to *Pf4cre*.
(D) Quantification of laminin surface coverage per megakaryocyte (in %, 17<n<19 as indicated in the bars, ***P>0.001 unpaired t-Test), (Middle) expression profile of the laminin staining along straight-lines (25 µm long) visible as white lines in the confocal images, and (Right) quantification of mesh sizes (in µm, 14<n<16, **P<0.01 Mann-Whitney).
*, sinusoid lumen; MFI, mean fluorescence intensity; MK, megakaryocyte; pm, plasma membrane; Bars, 10 µm.

Further confocal and immunoEM examination revealed a decrease in the expression of fibrillar fibronectin around *Itgb1*$^{-/-}$/*Itgb3*$^{-/-}$megakaryocytes, along with mislocalization of fibrinogen in the extracellular space of the DMS instead of the granules (**Suppl. Figures 3G and 3H**). These findings show that megakaryocytes, through β1 and β3 integrins dependant mechanisms, participate in their ECM microenvironment remodelling (ECM cage and fibronectin, fibrinogen deposition) and that megakaryocytes β1 and β3 integrins are required.

Normal ECM organization is essential for proper megakaryocyte intravasation

Next, we investigate the relevance of the ECM cage to platelet and megakaryocyte functions. Flow cytometry showed that *Itgb1*$^{-/-}$/*Itgb3*$^{-/-}$platelets have intact α-granule secretion but impaired integrin-mediated aggregation, consistent with the bleeding phenotype observed in these mice (Janus-Bell et al., 2024) (**Suppl. Figure 4A**). As we previously described that *Itgb1*$^{-/-}$/*Itgb3*$^{-/-}$ mice had a 50% reduction in platelet count (Guinard et al., 2023), we hypothesized that the organization of the ECM cage could contribute to the maturation process of megakaryocytes. Firstly, the number, ploidy, and maturation stages of megakaryocytes in *Itgb1*$^{-/-}$/*Itgb3*$^{-/-}$mice are similar to control mice. However, consistent with previous reports, these mutant megakaryocytes have a disorganized membrane system and smaller cytoplasmic areas compared to normal cells (**Suppl. Figures 4B-E**). We also analyzed megakaryocyte localization in the bone marrow tissue. We found a significantly higher proportion of megakaryocytes that were extending intravascular fragments (i.e., intravasation) in *Itgb1*$^{-/-}$/*Itgb3*$^{-/-}$ mice (15.1 ± 2.7% of total bone marrow megakaryocytes) compared to that in *Pf4Cre* mice (2.9 ± 0.4% of total megakaryocytes). More strikingly, intact megakaryocytes were found in the sinusoid lumen, a rare phenomenon in control mice under physiological conditions (**Figures 4A-B**).

To elucidate which of the two integrins was responsible for the observed phenotype, we employed single-knockout mice (**Figure 4C**). Analysis of the ECM cage revealed a trend towards decreased laminin Y1 density around *Itgb1*$^{-/-}$ megakaryocytes, while no notable changes were observed around *Itgb3*$^{-/-}$cells. No statistically significant increase in intravasation events was observed in either single knock-out mouse model. This suggests a redundant role of both integrins in regulating the megakaryocyte ECM cage and the intravasation process, potentially compensating for each other's role. Additionally, we investigate the role of GPVI, one of the two well-characterized collagen receptors in this process (**Figure 4C**), and no alterations in ECM cage formation or intravasation behavior were noticed, which is in agreement with previous reports (Semeniak et al., 2019).

To understand the unusual localization of circulating *Itgb1*$^{-/-}$/*Itgb3*$^{-/-}$megakaryocytes in the bloodstream, we used intravital 2-photon microscopy imaging to describe the dynamic of the megakaryocyte behavior. We used the GPIX marker, a subunit of the GPIb-V-IX complex that is expressed on mature megakaryocytes, to track the behavior of megakaryocyte in living mice. Among the stabilized megakaryocytes at the parasinusoidal interface, we could observe the cellular distortions of *Itgb1*$^{-/-}$/*Itgb3*$^{-/-}$ megakaryocytes and their exit of the marrow (**Figures 4D-E**, movie 3). Flow cytometry analysis did not allow us to detect intact megakaryocytes in the blood in *Itgb1*$^{-/-}$/*Itgb3*$^{-/-}$blood samples (**Suppl. Figure 4F**). However, large megakaryocyte nuclei were observed within the downstream pulmonary capillaries of these mice (**Figures 4F-G**), suggesting that circulating megakaryocytes in *Itgb1*$^{-/-}$/*Itgb3*$^{-/-}$mice are in large proportion retained in lung microvasculature shortly after entering the bloodstream. Transmission electron microscopy (TEM) observation confirmed that intact *Itgb1*$^{-/-}$/*Itgb3*$^{-/-}$ megakaryocytes were similar in size and ultrastructure to those in the stroma compartment (**Figure 4H**). Furthermore, no significant change in the size of the endothelial pores (*Itgb1*$^{-/-}$/*Itgb3*$^{-/-}$: 4.6 ± 0.3 µm; *Pf4Cre*: 4.3 ± 0.4 µm) was observed, indicating that increased megakacaryocyte intravasion in not link to endothelium alteration in mutant mice.

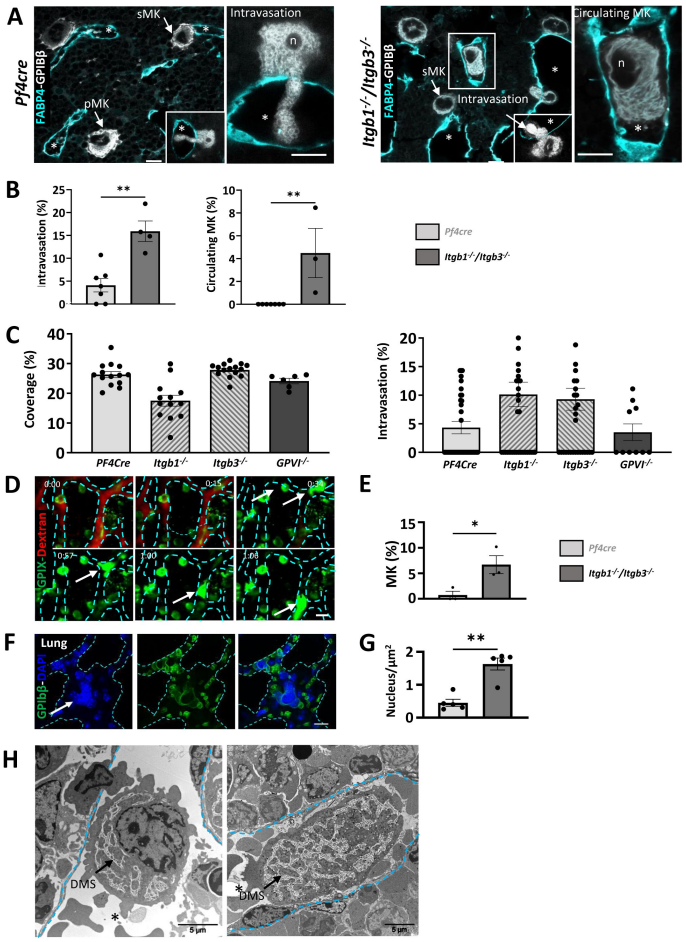

Figure 4

Integrins protects megakaryocytes from entering the bloodstream as whole cells

(A-C)) Higher proportion of intravasation events in mice lacking β1/β3 integrins.
A. Representative confocal images of *Pf4cre* and *Itgb1*$^{-/-}$*/Itgb3*$^{-/-}$whole-mount bone marrow immunostained for GPIbβ (white) and FABP4 (cyan).
B. Quantification of megakaryocyte intravasation and circulating megakaryocytes (3 mice minimum for each genotype, 213<n<397 for Pf4cre and *Itgb1*$^{-/-}$*/Itgb3*$^{-/-}$, ** P<0.001 Mann Whitney).
C. Quantification of the laminin γ1 deposition in the ECM cage in single knockout integrins and in GPVI knockout. Quantification of the intravasation events in single knock-out mice showing that both integrins are essential for the proper anchoring of megakaryocytes in their vascular niche.
(D -E) Intravital two-photon imaging of *Itgb1*$^{-/-}$*/Itgb3*$^{-/-}$ mouse calvarial bone marrow
D. Tissues were stained with intravenously injected AF488-conjugated anti-GPIX antibody and rhodamin dextran. The white arrow indicates an intrasinusoidal *Itgb1*$^{-/-}$*/Itgb3*$^{-/-}$megakaryocyte, dotted lines illustrate the sinusoid wall and the values in the left corner show the time-lapses.
E. Quantification of circulating megakaryocytes, expressed as a percentage of the total number of megakaryocyte (from 3 independent experiments, 130<n<136, 0.0279 *P<0.1, Paired t-test).
(F-G) Large megakaryocyte nuclei detected in the pulmonary capillaries of *Itgb1*$^{-/-}$*/Itgb3*$^{-/-}$ mice
F. Representative confocal images showing megakaryocytes' nucleus (arrow, GPIbβ green, DAPI nucleus) within the pulmonary microvessels of *Itgb1*$^{-/-}$*/Itgb3*$^{-/-}$ mice. Cyan dotted lines indicate the vessel wall.
G. Quantification of the intravascular megakaryocytes (from 5 independent experiments, 28<n<149, 0.0079 ***P*<0.01, Mann-Whitney).
(H) Two TEM image showing intravascular entire *Itgb1*$^{-/-}$*/Itgb3*$^{-/-}$ megakaryocyte.
*, sinusoid wall; FG, fibrinogen; FN, fibronectin; FG, fibrinogen; n, nucleus; sMK, sinusoid-associated MK; pMK, MK in the parenchyma; PPT, proplatelets; Bars in A-G, 10 µm; Bar in E, 5 µm; Bar in G, 30µm.

Integrins promote megakaryocyte adhesion to the ECM components of the bone marrow

We next assessed the contribution of integrins adhesive function in megakaryocyte anchorage to ECM. Under static conditions, most *Itgb1*$^{-/-}$/*Itgb3*$^{-/-}$megakaryocytes did not spread and still showed a round shape on immobilized laminin, fibronectin or fibrinogen (**Figures 5A-B**). We next measured the adhesive potential of freshly isolated bone marrow megakaryocytes to test for such an adhesive role. To this end, we used a miniaturized microfluidic-based experimental model in which individual megakaryocyte detachment was tracked when exposed to a flow rate of 300s-1, similar to the flow typically found in sinusoids (**Suppl. Figure 5A-B**). *Pf4-Cre* megakaryocytes had capture yields of 70.5% on laminin, 83.6% on fibrillar fibronectin, and 82.0% on fibrinogen. Laminin exhibited the least adhesion, emphasizing the importance of the molecular composition of the said 3D ECM cage and its evident impact on the adhesion response of megakaryocytes *in vivo* (**Figures 5C-D**). *Pf4-Cre* megakaryocytes remained anchored, while *Itgb1* $^{-/-}$/*Itgb3* $^{-/-}$ megakaryocytes experienced higher detachment rates across various ECMs (movies 4 and 5). In line with this conclusion, we used the bone marrow explant model to study the adhesion properties of the megakaryocytes associated with their 3D ECM cage (**Figures 5E-F**). This model enabled us to quantify the physical detachment of megakaryocytes at the periphery of the explants. After 3 hours, more megakaryocytes detached from *Itgb1*$^{-/-}$/*Itgb3*$^{-/-}$bone marrow tissue than *Pf4-Cre* explants, reaching a plateau at 6 h. These findings indicate that β1 and β3 integrins control ECM-megakaryocyte interactions in their native bone marrow microenvironment.

Collectively, our results highlight the essential roles of β1 and β3 integrins in forming 3D ECM cages around megakaryocytes and modulating their adhesion within the bone marrow, which helps stabilize the cells in their vascular niche and prevent the passage of intact megakaryocytes through the sinusoid barriers.

Cage compression via metalloproteinase inhibition affects the maturation of megakaryocytes

Our results suggest that a weakened ECM cage promotes megakaryocyte intravasation through reduced adhesion. We, therefore, tested whether an increase in cage density also may affect megakaryocyte functions. For that purpose, we proposed to decrease the catabolic aspect occurring in the ECM equilibrium between its synthesis and degradation. To this aim, mice were injected with batimastat (30 mg/kg) and ilomastat (20 mg/kg) for 7 days, in order to inhibit the activation of MMPs in the megakaryocyte microenvironment (Winer et al., 2018) (**Supplemental Figure 6A**). These mice produced platelets normally in terms of both count and average platelet function (**Suppl. Figures 6B-C**). Regarding the cage, this treatment increased the ECM density in megakaryocyte surrounding, as evidenced by reduced fiber length and pore size (**Figures 6A-B**).

We investigated whether this denser ECM cage might affect megakaryopoiesis. Remarkably, treatment with MMP inhibitors resulted in a significantly higher proportion of smaller megakaryocytes compared to untreated mice (white arrows in **Figures 6C-D**). To better evaluate the extent of this defect, we employed TEM (**Figure 6E**). We found that 53.7% of the megakaryocytes lacked the appropriate organization of the DMS in MMP inhibitors-treated mice, reflecting a primary failure in the cytoplasmic maturation (Stage II in **Figure 6F** right). To determine whether MMP inhibition could directly affect megakaryocytes, we cultured primary megakaryocytes in the presence of increasing concentrations of inhibitors. We found no significant change in their proliferation, maturation, and proplatelet formation (**Suppl. Figure 6D**). Although these *in vitro* system and exogenous MMPs may not fully recapitulate the complexity of the bone marrow situation, these findings suggest that disturbing ECM remodelling significantly impacts megakaryocyte maturation.

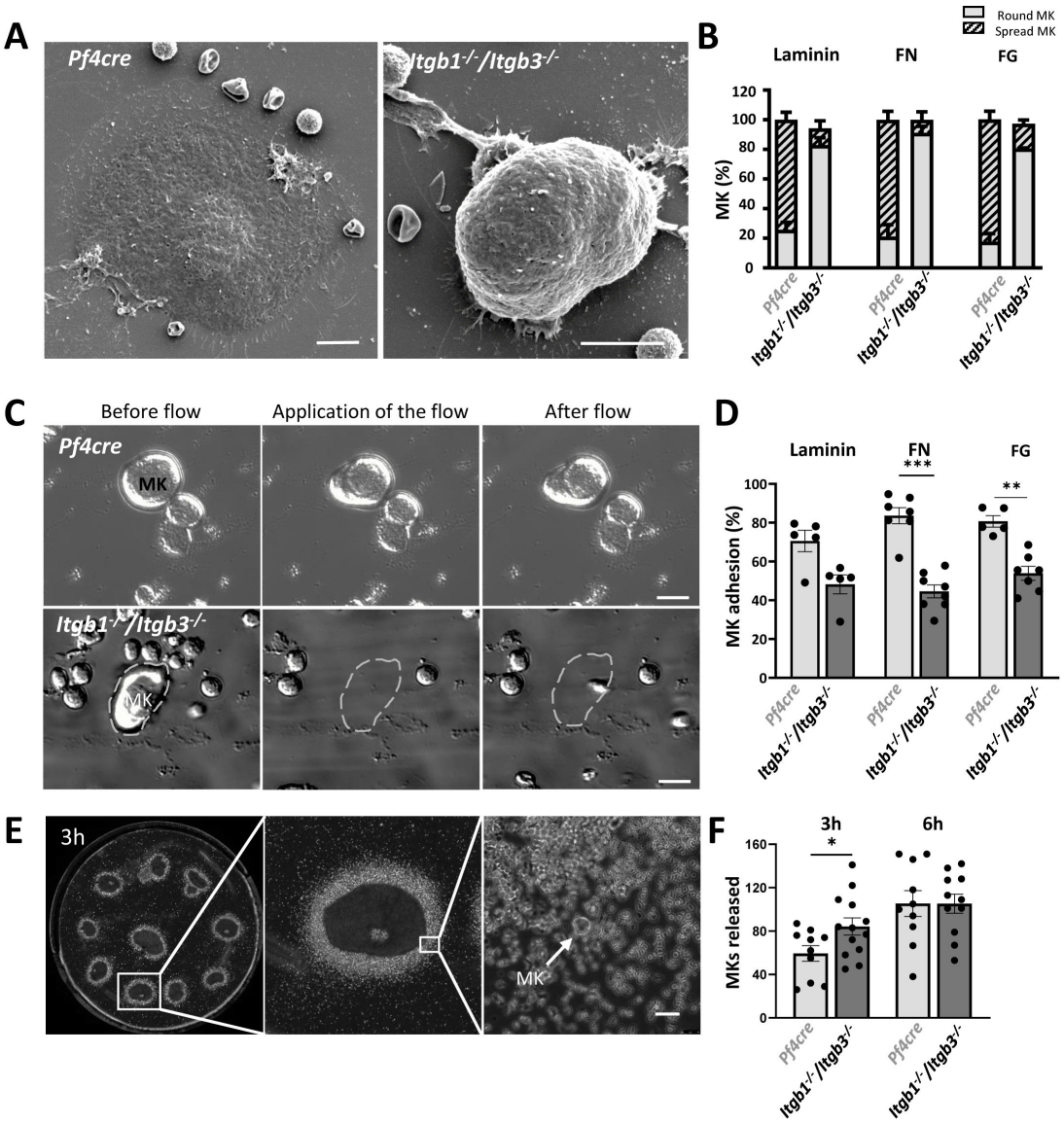

Figure 5

Integrins promote megakaryocyte adhesion to the ECM components of the bone marrow

(A-B) Impaired adhesion and spreading of *Itgb1*$^{-/-}$*/Itgb3*$^{-/-}$ megakaryocytes.
A. Representative SEM images depicting bone marrow-derived megakaryocytes adhering on laminin.
B. Spreading (hatched bars) and round (grey bars) megakaryocytes were counted following 3h incubation on laminin, fibronectin (FN), and fibrinogen (FG) (in %) (from 4-6 independent experiments).
(C-D) Microfluidic flow chamber to study megakaryocyte adhesion efficiency.
C. Representatives bright field images showing that upon flow application, *Itgb1*$^{-/-}$*/Itgb3*$^{-/-}$ megakaryocytes detach from fibrillary fibronectin protein, while *Pf4Cre* MKs remain attached.
D. Quantification of the detachment of *Pf4cre* and *Itgb1*$^{-/-}$*/Itgb3*$^{-/-}$ megakaryocytes on laminin, fibrillar fibronectin and fibrinogen (from 5 to 7 independent experiments,**P<0.01, ***P<0,001, Mann-Whitney).
(E-F) Reduced physical anchoring of *Itgb1*$^{-/-}$*/Itgb3*$^{-/-}$ megakaryocytes to bone marrow.
E. Representatives bright field images of the ten femur bone marrow sections placed in an incubation chamber (left panel), of the box (center panel) and of the megakaryocytes released from the periphery of the explants (right panel).
F. Quantification of the number of *Pf4cre* and *Itgb1*$^{-/-}$*/Itgb3*$^{-/-}$ megakaryocytes released from the explants following 3h (from 10 to 13 independent experiments, 594<n<1095 for Pf4cre and *Itgb1*$^{-/-}$*/Itgb3*$^{-/-}$, *P<0.05, unpaired t-test).
dotted lines, MK detachment; MK, megakaryocytes, FN, fibronectin; FG, fibrinogen; n, number of cells studied; Bars in A, 10 µm; Bars in B, 20 µm; Bars in B, 30 µm.

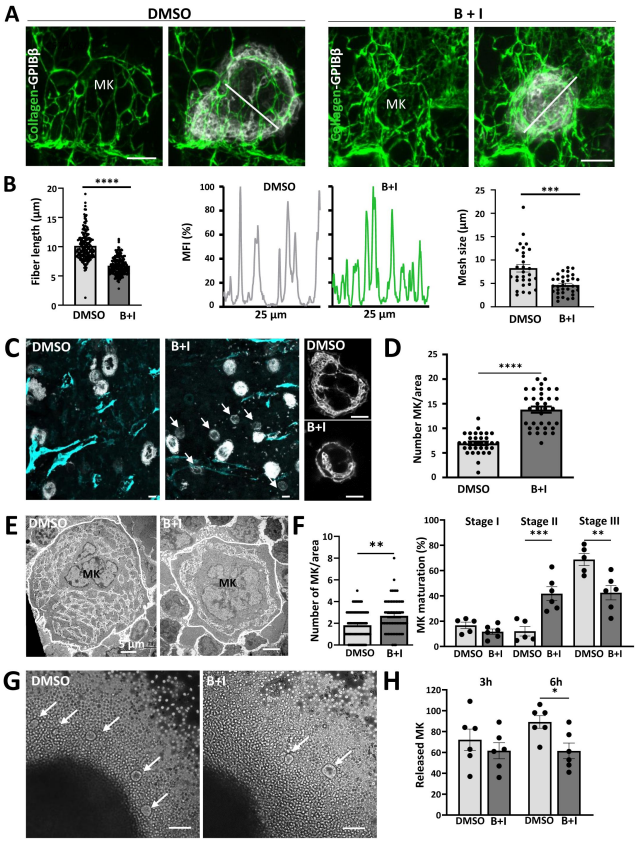

Figure 6

Maturation of the 3D ECM cage is correlated with maturation of the DMS in megakaryocytes

(A-B) MMP inhibition leads to a densification of the 3D ECM cage.
A. Representative 3D confocal images showing a significant increase in collagen IV deposition (green) on the megakaryocyte surface in treated mice treated with the intravenous cocktail of protease inhibitors (B + I).
B. (Left) Quantification of collagen IV fluorescence showed a shortening of collagen IV fibers in treated mice compared to that in control mice (from 3-5 independent experiments, 20<n<22 as indicated in the bars, ****P<0;001, Mann-Whitney), (Middle) Histograms of fluorescence intensity versus distance showed an increase in cross-linking with a reduction in pore size (white lines of 25µm length are visible in the confocal images), (Right) Reduction in mesh sizes in treated mice (from 3 independent experiments, 7<n<12, ***P>0.001, t-test).
(C-D) MMP inhibition affects megakaryocyte growth.
C. Representative confocal images from DMSO *vs* B+I treated mice immunostained for GPIbβ (white) and FABP4 (cyan), zoomed-in images showing the difference in megakaryocyte size between the two groups (arrows).
D. Quantification of the number of megakaryocytes per bone marrow area (194 x 194 µm) (from 3 independent experiments, 229<n<483 as indicated in the bars, ****P<0.0001, Mann-Whitney).
(E-F) MMP inhibition leads to an increased in the number of immature megakaryocytes.
E. TEM observation revealed the presence of numerous immature megakaryocytes (stage II) in treated mice as compared to fully mature megakaryocytes in control mice (stage III).
F. Quantification of the total number of megakaryocytes (145<n<169 as indicated in bars, **P<0.01, Mann-Whitney) and in the proportion of immature megakaryocytes (stage II) in the B + I group (from 3 independent experiments, **P < 0.05, ***P < 0.01, one way ANOVA with Tukey correction).
(G-H) MMP inhibition reduced release of megakaryocytes from the bone marrow explant.
G. Representatives bright field images of the megakaryocytes (arrows) released from the periphery of the control and treated explants.
H. Quantification of the number of megakaryocytes released following 3h and 6h (from 6 independent experiments, 369<n<783 for DMSO and B+I, *P<0.05, unpaired t-test).
B + I, batimastat + Ilomastat; sMK, sinusoid-associated MK; pMK, MK in the parenchyma; n, number of cells studied; Bars in A and C, 10 µm; Bars in E, 5 µm; Bar in G, 50 µm.

An additional phenotype associated with a denser ECM environment is a significant increase in the total megakaryocyte number in MMP inhibitor-treated mice compared to the control condition (**Figures 6D** and **6F** left). Moreover, immunofluorescence analysis of bone marrow sections revealed an upregulation of activated β1 integrin (**Suppl. Figure 6E**). These results indicate that increased ECM density may promote megakaryocyte adhesion within the congested microenvironment of the bone marrow. To further investigate this point, we quantified the number of megakaryocytes released from bone marrow explants. We observed a significant reduction in megakaryocyte egress from the bone marrow microenvironment after 6 h in MMP inhibitor-treated compared to control mice (**Figure 6G-H**). Together, these results indicate that MMPs are essential regulators of ECM homeostasis within the bone marrow, influencing megakaryocyte maturation and attachment to the vascular niche.

Discussion

Physiological platelet formation relies on the strategic positioning of mature megakaryocytes at sinusoids to facilitate polarised proplatelet extension and platelet release into circulation. This study identifies a 3D ECM cage anchoring megakaryocytes to bone marrow sinusoids. This cage, composed of laminin γ1 and α4 and collagen IV fibers, extends from the basement membrane and surrounds megakaryocytes. Megakaryocyte integrin signaling and ECM proteolysis regulate its remodeling and adhesive properties. This dynamic microenvironment is key for megakaryocyte positioning, maturation, and intravasation into the bloodstream, representing a novel concept in understanding physiological platelet formation (Graphical Abstract, **Figure 7**).

In line with previous studies (Guinard et al., 2023; Larson & Watson, 2006; Malara et al., 2014; Semeniak et al., 2016), we identified the presence of collagen IV, laminin γ1, fibronectin, and fibrinogen surrounding sinusoid-associated megakaryocytes. Notably, when analyzed using immunofluorescence and transmission electron microscopy (TEM), collagen I fibers were absent under steady-state conditions. The discrepancy between our results and those reported in the literature may be attributed to differences in staining methodologies or variations in the physiological context of the bone marrow. Furthermore, our findings indicate that GPVI-deficient megakaryocytes do not display alterations in ECM cage formation, vessel association and intravasation behavior. These observations support studies showing GPVI and α2β1 integrins are not critical for megakaryocyte function, underscoring potential redundancy in ECM-receptor interactions (Semeniak et al., 2019). Besides, non-protein ECM molecules, including glycosaminoglycans, have been shown to play an essential role in supporting megakaryocyte function, including maturation (Petrey et al., 2016; Piszczatowski et al., 2022; Vögtle et al., 2019).

We identify laminin and collagen IV as the principal structural components of this ECM cage. Consistent with previous research (Abbonante et al., 2016; Cai et al., 2022; Susek et al., 2018), these ECM proteins were detected intracellularly within megakaryocytes and in stromal cells situated in their vicinity. This indicates that the ECM cage proteins may be derived from autocrine synthesis and their production by neighbouring cells. Interestingly, while fibronectin and fibrinogen were found around megakaryocytes, they do not form a ECM cage, suggesting distinct functional roles, potentially related to megakaryocyte expansion in bone marrow fibrosis (Malara et al., 2019; Matsuura et al., 2020).

Our findings in *Lamα4*-deficient mice reveal that the ECM cage is critical for positioning megakaryocytes near sinusoids. It is established that CXCL12 is a most potent physiological chemoattractant for megakaryocytes and that the parasinusoidal location of megakaryocytes in the bone marrow is mediated by the CXCL12/CXCR4 interaction (Hamada et al., 1998; Wang et al., 2019). Other chemoattractive factors also include fibroblast growth factor 4 (FGF4) (Avecilla et al., 2004) and VWF (Ouzegdouh et al., 2018). Besides its potential role as a reservoir of such

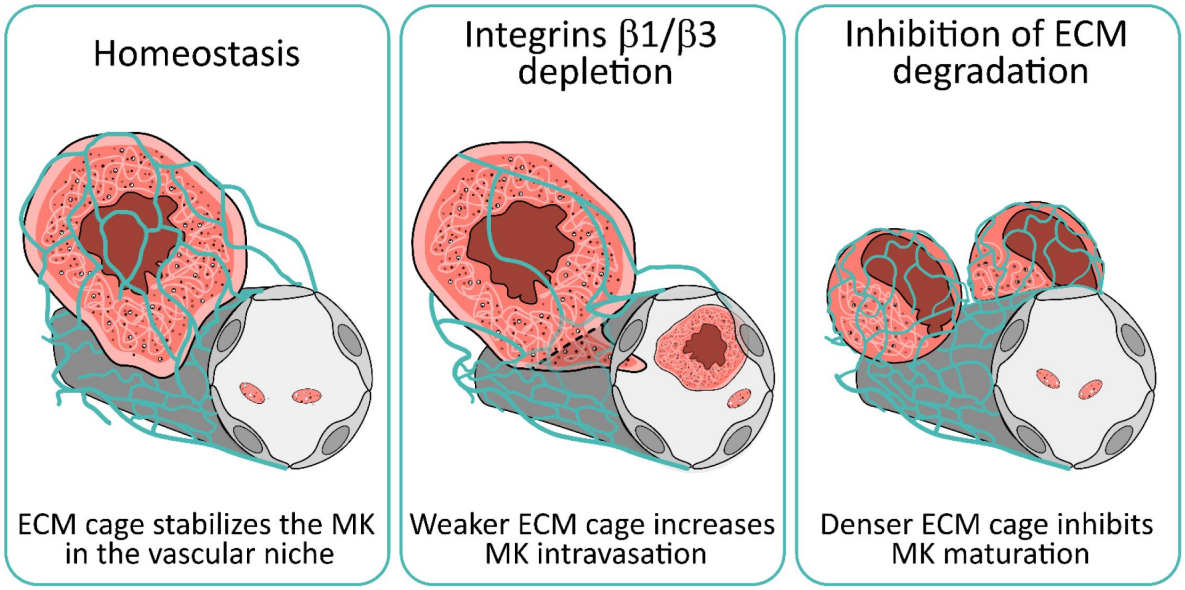

Figure 7

Integrin-mediated signaling and MMP proteolysis regulate the matrix remodeling and the adhesive properties of the 3D ECM cage, which control megakaryocyte maturation and intravasation at the bone marrow-blood interface.

growth factors, we show that the ECM cage is also a crucial element in maintaining megakaryocytes in the proximity of sinusoids, which is essential for their efficient maturation and optimal platelet production. We also find the persistent presence of this ECM cage throughout megakaryocyte maturation, supporting previous findings that megakaryocyte development occurs primarily at the sinusoid (Gaertner et al., 2024; Lichtman et al., 1978; Stegner et al., 2017).

Our study highlights the indispensable roles of β1 and β3 integrins in maintaining megakaryocyte stability within the vascular niche. We demonstrate that these integrins are crucial for two fundamental processes : (1) the building of the 3D ECM cages, and (2) the ECM-mediated adhesion mechanisms to the vascular niche. Integrins biochemical and mechanical signal transduction play key roles in ECM remodelling (Larsen et al., 2006) and can generate the forces that may cause these changes (Lemmon et al., 2009). For instance, RhoA inhibition in *Itgb1*$^{-/-}$/*Itgb3*$^{-/-}$ megakaryocytes (Guinard et al., 2023) is likely contributing to the altered ECM remodeling. Nevertheless, we still need to understand how in megakaryocyte β1 or β3 integrins participate in ECM remodelling and ECM cage dynamics. Our work further demonstrates that in these mice, intact megakaryocytes can enter the general circulation. Of note, no intravascular megakaryocytes were found in *Lamα4*-deficient mice, which have a normal collagen IV cage but a compromised laminin cage. This indicates that integrity of all components of the cage is not needed to keep megakaryocytes from entering circulation. Importantly, circulating megakaryocytes have also been observed in humans during emergency megakaryopoiesis, such as in cases of infectious diseases, inflammatory conditions, and following cardiopulmonary bypass procedures (Frydman et al., 2023; Gelon et al., 2022; Puhm et al., 2023; Rapkiewicz et al., 2020). These circulating megakaryocytes have been implicated in thrombotic complications, underscoring the importance of integrin signaling-dependent mechanisms regulating megakaryocyte retention and release.

The precise role of the ECM cage in platelet production remains incompletely understood. In the Lamα4$^{-/-}$ mice, a collagen-rich ECM cage persists with normal fibronectin deposition, whereas the *Itgb1*$^{-/-}$/*Itgb3*$^{-/-}$ model displays a much more severe phenotype, characterized by the loss of both the laminin cage and collagen, along with the absence of fibrillar fibronectin. The preserved collagen and fibronectin in Lamα4$^{-/-}$ mice may allow for residual activation of signaling pathways - potentially through integrins or alternative mechanisms - compared to the *Itgb1*$^{-/-}$/*Itgb3*$^{-/-}$model, where these matrix components are absent.

MMPs profoundly influence megakaryocyte maturation and their association with the vascular niche by modulating the density of ECM cage architecture. This finding highlights the dynamic nature of the bone marrow microenvironment and its impact on megakaryopoiesis. Dysregulation of ECM production, often associated with bone marrow pathologies, can lead to its uncontrolled accumulation. In myelofibrosis, for instance, megakaryocytes secrete transforming growth factor-β1 (TGF-β1) which stimulates excessive ECM production by stromal cells (Abbonante et al., 2016). This pathological ECM accumulation leads to abnormally smaller megakaryocytes that exhibit reduced platelet production (Gianelli et al., 2023; Malara et al., 2018; Sarachakov et al., 2023). Likewise, we observed smaller and immature megakaryocytes retained in the constrained ECM microenvironment of the bone marrow, associated with an upregulation of activated β1 integrin in treated mice. Interestingly, previous research by K. Hoffmeister's group has demonstrated that proper megakaryocyte localization at the sinusoids depends on β1 integrin glycosylation. Specifically, the absence of galactosylation in β4galt1$^{-/-}$ megakaryocytes leads to hyperactivity of β1 integrin, which negatively impacts the formation of the DMS (Giannini et al., 2020). Building on these insights, our study shows the coordinated interplay between integrin-mediated signaling and MMP proteolysis, working together to tightly regulate the density and cross-linking properties of the ECM cage and thereby control megakaryocyte maturation at the bone marrow-blood interface. Intriguingly, despite these effects on megakaryocyte maturation, we

observed no significant changes in circulating platelet counts, and importantly, platelet function remained preserved. This supports the idea that differences in ECM composition can influence the signaling environment and megakaryocyte maturation, but do not fully abrogate platelet function.

The influence of ECM features - like fiber length and pore size - on megakaryocyte biology is complex and not yet fully understood. Longer ECM fibers may help cells adhere better (Barriga et al., 2018; Dolega et al., 2021). Larger pores could make it easier for megakaryocytes to mature and to extend proplatelets at the bone marrow-blood interface. Also, the mechanical properties of the ECM, particularly its stiffness, have emerged as critical environmental determinants of megakaryocyte development and function (Abbonante et al., 2017; Aguilar et al., 2016; Guinard et al., 2023; Leiva et al., 2018). Notably, megakaryocytes possess mechanosensing capabilities, primarily mediated by the β3 integrin subunit, enabling them to detect and respond to changes in substrate stiffness (Guinard et al., 2023). The assembly of extracellular matrix (ECM) fibronectin around megakaryopoiesis involves a more complex interplay of integrins, with both β1 and β3 integrins playing essential roles in fibrillogenesis (Abbonante et al., 2024; Guinard et al., 2023). This cooperative relationship appears to be conserved across various cell types (Attieh et al., 2017; De Mets et al., 2019; Kyumurkov et al., 2023). This may explain why the deletion of both integrins is required to affect the 3D ECM cage and megakaryocyte behavior significantly. We can not exclude that other ECM ligands of β3 integrins, such as fibronectin, may contribute to the organization of collagen IV and laminin, influencing the overall architecture of the vascular niche (Petito & Gresele, 2024; Yang et al., 2022; Zeng et al., 2018). Indeed, it is known that the fibronectin matrix favors the deposition of other ECM proteins, such as collagens IV and various other glycoproteins (Saunders & Schwarzbauer, 2019). This hypothesis underscores the need for further investigation into the spatio-temporal dynamics of ECM component assembly in the megakaryocyte vascular niche.

Overall, our findings reveal the supportive role of the ECM cage in platelet biogenesis. Integrin-mediated ECM interactions are clearly crucial, as demonstrated by the 50% reduction in platelet counts observed in integrin double knockout mice. In summary, the ECM cage acts as a finely tuned facilitator, optimising the efficiency and precision of platelet production by guiding megakaryocytes to the right place at the right time.

Material and methods

Animals

We used wild type (WT) mice (C57BL/6J from C. River, L'Arbesle, France), Itgb1$^{-/-}$/Itgb3$^{-/-}$ double knock out mice and Pf4cre mice aged 10 to 15 weeks. Pf4cre mice expressed the Cre recombinase under the control of the Pf4 promoter. The β1$^{fl/fl}$ (Potocnik et al., 2000) and β3$^{fl/fl}$ (Morgan et al., 2010) mice were crossed with mice expressing the Cre recombinase under the control of the Pf4 promoter to obtain inactivation in the MK lineage. *Itgb1*$^{-/-}$*/Itgb3*$^{-/-}$double knock out (KO) mice were crosses of the two single KO lines, as described in Guinard et al., 2023. *GPVI* $^{-/-}$ mice and *Lamα4*$^{-/-}$ mice were from Nieswandt and Qian labs (Bender et al., 2011; Cai et al., 2022). All animal studies were approved by the French legislation for animal experimentation and in accordance with the guide for the care and use of laboratory animals as defined by the European laws (Animal Facility Agreement C- 67-482-10).

Chemicals

Dimethyl sulfoxide (2438), bovine serum albumin (900.011), saponin (47036), Triton X-100 (T8787), fibrinogen and batimastat (SML0041) (Sigma-Aldrich, Rueil-Malmaison, France), Ilomastat (GM6001, HY-15768) (MedChemExpress, Clinisciences, France), Dulbecco's modified Eagle's medium (DMEM), penicillin, streptomycin, and glutamine (Invitrogen, Cergy-Pontoise, France),

Gelatin-Oregon Green 488 conjugate (G-13186) (Life Technologies), Laminin 511 recombinant (Biolamina) and fibronectin from human plasma from (341635, Calbiochem) were used in this study.

Antibodies

See **Tables 1** and **2** in "Data Supplements" for details.

GPIX and GPIbβ are components of the GPIb-IX complex, identifying mature megakaryocytes (Lepage et al., 2000). The choice of marker used to identify megakaryocytes in different experiments is primarily based on technical considerations. Intravital experiments have been standardised using AF488-conjugated anti-GPIX to consistently identify mature megakaryocytes. The rest of the manuscript uses GPIbβ (GP1bβ) due to its strong, specific, bright staining.

Extrusion and Preservation of Murine Bone Marrow

Bone marrow extrusion, without leaving any residual bone, was obtained by carefully flushing the femurs of mice with PBS using a 21-gauge needle attached to a 10 mL syringe (see photo in **Figure 1D**) (Scandola et al., 2021). To maximize the preservation of the bone marrow integrity, we used a double fixation procedure (4 % paraformaldehyde and 0.4% glutaraldehyde for 1 hour) immediately after bone marrow extrusion, followed by embedding it in 4 % low-melting-point agarose to preserve as much as possible their three-dimensional architecture.

Isolation of freshly isolated bone marrow-derived megakaryocytes

Bone marrow megakaryocytes were dissociated using a 21G needle and filtered through a 40 µm Millipore filter. The filter was then rinsed in DMEM + 1% fœtal bovine serum, and the isolated megakaryocytes were adjusted to 300 cells/ml in the same medium.

2D confocal microscopy on bone marrow cryosections

This study explores the interactions between megakaryocytes and their immediate ECM microenvironment. Ultrathin cryosections were used for their superior axial resolution, offering a 2- to 3-fold improvement over conventional confocal microscopy, which facilitates analysis of signal superposition. Cryosections from WT extruded bone marrow were used to study the ECM composition and distribution of sinusoid-associated megakaryocytes. Bone marrow was fixed in a mix of 2 % paraformaldehyde-0.2 % glutaraldehyde in 0.2 M sodium cacodylate buffer for 1 hour. The fixed samples were infiltrated with 2.3 M sucrose and frozen in liquid nitrogen. Ultrathin cryosections of 250 nm were obtained at −110°C with a LEICA Ultracut UCT cryo-ultramicrotome (Leica Microsystems). For immunofluorescence staining, cryosections were labeled with primary antibodies and conjugated-second antibodies of the appropriate species and DAPI, as reported in **Table 1**. They were examined under a confocal microscope (TCS SP8, Leica) using the 63x objective with a numerical zoom of 4 (pixel size: 0.09µm). The bone marrow specimens from 3 mice were examined under identical conditions, using constant exposure and the same irrelevant antibodies. No fluorescence was detected using isotype-specific control IgG.

3D confocal analysis on bone marrow vibratome sections

Whole-mount bone marrow preparations were used to investigate i) the localization of megakaryocytes in the bone marrow and the lung and ii) the spatial organization of ECM around sinusoid-associated megakaryocytes. Megakaryocytes were classified based on their maturation stage: stage I (presence of granules, no clear DMS visible), stage II (developing DMS not yet organized), and stage III (DMS organized in platelet territories). Mice from each genotype were analyzed and image acquisitions were performed in a blinded manner.

Antigen	Origin and isotype	Reference and supplier	Cryosections	Whole-mount
Primary antibody				
Collagen I	Rabbit polyclonal	Chemicon (Merck) ab765p	5µg/ml	
Collagen III		Invitrogen PA5-34787	10µg/ml	
Collagen IV		Chemicon (Merck), ab756p	5µg/ml	
FABP4	Goat polyclonal	R&D Systems AF1443	0.5µg/ml	
Fibrinogen	Rabbit polyclonal	Dako (Glostrup, Denmark), A0080	10µg/ml	
Fibronectin		ab2413 (Abcam ; Paris, France)	10µg/ml	
GPIbβ	Rat monoclonal	In house (Strasbourg, France)	1/300	1/300
Activated β1 integrin (9EG7)		553715 (BD Pharmingen)	10µg/ml	
Pan-laminin	Rabbit polyclonal	L9393 (Sigma-Aldrich)	10µg/ml	
Von Willebrand Factor		Dako, A0082	10µg/ml	
β1 integrin (MB1.2)	Rat monoclonal	Merck, MAB1997	10µg/ml	
LucA5	Rat IgG2A monoclonal	Emfret analytics, LucA5	10µg/ml	
Secondary antibody				
AF488-anti-rabbit immunoglobulin	Donkey	A21206 (Invitrogen)	1/150	
AF488-conjugated anti-rabbit immunoglobulin	Goat	A11070 (Invitrogen)		
AF647-conjugated anti-rabbit immunoglobulin	Goat	A21245 (Invitrogen)		
AF647-conjugated anti-rat immunoglobulin	Goat	A21247 (Invitrogen)		
AF555-conjugated anti-goat immunoglobulin	Donkey	A21432 (Invitrogen)		
AF647-conjugated anti-pan-laminin	Rabbit	In house	25µg/ml	
AF555-conjugated anti-collagen IV	Rabbit	In house	30µg/ml	
AF647-conjugated anti-GPIX antibody	Rat	nXiaB4 Emfret		

Table 1

Antigen	Origin and isotype	Reference and supplier	Fluorophor	Flow cytometry	Whole-mount
Conjugated antibody					
JONA Activated integrin αIIbβ3	Rat IgG2b	Emfret analytics M023-2	PE	Dilution of 1/5	
P-selectin (CD62P)	Mouse IgG2a, κ	BioLegend 148303	APC	1 µg/mL	
CD45 (clone 30-F11)	Rat IgG2b, κ	eBiosciences 12-0451-82	PE-A	1 µg/mL	
TER119	Rat / IgG2b, κ	eBiosciences 17-5921-82	APC-A	1 µg/mL	
GPIbβ	Rat monoclonal	In house (Strasbourg, France)	A647, A568, A488	1 µg/mL	
Hoechst-33342		Invitrogen H3570			10 µg/mL
Integrin αIIb (CD41 – clone MWReg30)	Rat IgG1 κ	eBiosciences 25-0411-82	PE-Cy7	1 µg/mL	

Table 2

For megakaryocyte localization, sections of femurs's bone marrow or lungs fixed in 2% paraformaldehyde and 0.2% glutaraldehyde for 1 hour, with a thickness of 250 µm, were incubated with FABP4 overnight. This was followed by overnight staining with Alexa 568-conjugated anti-GPIbβ antibody and Alexa 488 Donkey anti-Goat for FABP4. Finally, Hoechst 33342 was used for counterstaining for 10 minutes. The fluorescently labeled tissue was placed cut-face down into incubation chambers and mounted with Mowiol mounting solution. The Leica SP8 confocal microscope was used to collect a series of x-y-z images. The images were typically 194×194 µm x-y size and were collected along the z-axis at 1 µm step size through 50 µm of bone marrow tissue. The 40x objective with a numerical zoom of 4 (pixel size: 0.142 µm) was used. The lung was imaged using an x63 objective with a 2.5 digital zoom (pixel size: 0.145 µm).

To perform 3D ECM analysis, bone marrow samples were fixed in 4% PFA and 0.4% GA for 1 hour, then embedded in 4% agarose and cut into 250 µm-thick sections using a vibratome. These sections were then incubated overnight at 4°C with primary antibodies targeting laminin, type IV collagen, fibronectin, and fibrinogen, followed by corresponding secondary antibodies and Hoechst 33342 counterstaining. Series of x-y-z images of typically 46.13*46.13 µm x-y size were collected along the z-axis at 1 µm step size through 15-35 µm of sinusoid-associated megakaryocytes, using the 63x objective with a numerical zoom of 4 (pixel size: 0.09) from a Leica SP8 confocal microscope. For quantitative spatial analysis of ECM around megakaryocytes, the observations have been made on z-stacks as described by *Voisin et al.* (Voisin et al., 2010).The fluorescence was delineated on the maximum z-stack projection of half a megakaryocyte using Image J software.

Image processing to perform quantitative analyses of fluorescence profiles and fiber length are explained in **Suppl. Figure 7**. The random length measurement method uses random sampling to provide unbiased data on laminin/collagen fibers in a 3D cage. Measurements included intervals between different branching points throughout the cage, including branch ends. Processing involved five steps: 1) acquiring 3D images, 2) projecting onto 2D planar sections, 3) selecting random intersection points for measurement, 4) measuring intervals using ImageJ software, and 5) repeating the process for a representative dataset. Briefly, a binary threshold mask (0 for the background and 1 for the ECM network, threshold to reduce signal noise) was generated from the channel showing labeled collagen or laminin. The mask was then applied to the channel showing megakaryocytes, resulting in an image that corresponded to only an active ECM signal that colocalized with megakaryocytes. The mask was then applied to the collagen/laminin channel to determine the amount of fluorescent ECM within the mask. This enabled the determination of the cell area and the elimination of the signal outside the mask.

Intravital imaging

Pf4cre and *Itgb1*$^{-/-}$*/Itgb3*$^{-/-}$ mice underwent intravital imaging. To visualize megakaryocytes and sinusoids, an AF488-conjugated anti-GPIX antibody derivative and Texas Red dextran 70kDa were intravenously injected, respectively. The skull bone marrow was observed using two-photon microscopy, following the procedure described in reference (Bornert et al., 2021). The anesthetized mice were monitored for a maximum of 6 hours, during which one to four proplatelets were recorded. Two regions of interest were analyzed, each composed of 3 images (xyz = 1320 µm*1320 µm*100 µm, total volume/ROI = 0.17 µm3, pixel size = 0.867 µm at obj HC FLUOTAR L 25x/0.95 WATER zoom x1). A total of 130 megakaryocytes *PF4cre* vs. 130 megakaryocytes *Itgb1*$^{-/-}$*/Itgb3*$^{-/-}$ were analyzed and the results are expressed in %.

Electron microscopy

For Transmission electron microscopy, bone marrow was fixed in 2.5% glutaraldehyde for 1 hour and embedded in Epon as described (Scandola et al., 2021). Transversal thin sections of the entire bone marrow were cut and examined under a JEOL TEM (120 kV). The number of

megakaryocytes was counted per surface unit (s.u., 12,945 µm2). The observations from three independent mice were averaged.

For SEM, native bone marrow megakaryocytes were allowed to adhere to a surface coated with 300 µg/ml fibronectin, 100 µg/ml fibrinogen, or 50 µg/ml laminin 511. After gentle agitation to detach non-adherent cells, the remaining adherent cells were fixed in 2.5 % glutaraldehyde for 1 hour, dehydrated, attached to stubs, sputter coated, and examined under a Helios NanoLab microscope at 5kV (ThermoFisher, Eindhoven, The Netherlands). Adherent megakaryocytes where counted and classified as spreading or round cells. The results were obtained by the average from three independent mice.

Flow cytometry

Flow cytometry was used to investigate i) megakaryocyte ploidy, ii) intact megakaryocytes in the blood and iii) platelet activation.

For the ploidy analysis of the native megakaryocytes, mouse femurs, tibias, and iliac crests were harvested, cut into small fragments, and incubated in a PBS-collagenase-dispase mix (at 3 mg/mL and 4 mg/mL, 5mL/mouse respectively) for 30 min at 37°C. Then, the tube was filled with PBS-2% NCS to stop the collagenase, and the supernatant was 70 µm filtered to eliminate the bone fragments. After red cell lysis, the freshly isolated bone marrows were washed in PBS-2% NCS and stained with anti-CD41 and anti-CD42c antibodies and Hoechst. Anti Gr-1, B220, F4/80, and TER119 probes were used as a negative control to exclude granulocytes, B lymphocytes, macrophages, and erythrocytes from the total bone marrow suspension. The freshly isolated megakaryocytes were identified as a CD41/CD42c positive cell population and ploidy analysis was performed using Hoechst 33342. The results are representative of three independent experiments.

For detection of intact megakaryocytes in the blood, red blood cell lysis was performed using BD Lysing buffer solution according to manufacturer's instruction. The resulting mononucleated cells were labelled with fluorescent conjugated antibodies: anti CD41-PE-Cy7 (clone MWReg30), anti-CD42c-Alexa 488 (clone RAM-1), anti-CD45-PE (clone 30-F11), TER119-APC (clone TER119), antibodies from ebiosciences except RAM-1 antibody produced in house. Megakaryocytes enriched from bone marrow using BSA gradient were spiked into blood sample to validate the gating strategy to identify potential circulating megakaryocytes as $CD45^{+}TER119^{-}CD41^{+}CD42c^{+}$ events. 300.10^{3} $CD45^{+}TER119^{-}$ events were recorded. Data acquisition was performed on a Symphony A1 flow cytometer (BD Biosciences) and analyzed using BD FACS Diva Software (BD Biosciences).

For platelet activation studies, whole blood was collected from the tail vein and anticoagulated with hirudin (200 U /ml). Platelets were activated or not with collagen-related peptide (CRP, 40 µg/ml) and TRAP (4mM) for 15 min at 37°C and stained with FITC-labelled or 647-labelled rat anti-mouse GPIbβ and APC-labeled rat anti-mouse P-selectin or PE-labelled rat anti-mouse activated-αIIbβ3 antibodies. Fluorescence was quantified using an LSRFortessa cell analyze (BD Biosciences) and BD FACSDiva software. A total of 20.000 events were analyzed for each sample.

Microfluidic experiments

The PDMS microfluidic chamber channels were assembled and connected to a peristaltic pump, as described (Osmani et al., 2021). The channels were washed with PBS for 5 min and coated with laminin 511 (50 µg/ml), fibrillar fibronectin (300 µg/ml), or fibrinogen (100 µg/ml) overnight at 4°C, followed by a blocking stage with human serum albumin (1 %) for 30 min at RT. To produce fibrillar fibronectin, we use the method of mechanical stretching as described in Maurer et al, (Maurer et al., 2015). Freshly isolated megakaryocytes were seeded at a concentration of 30 cells /µL per channel and incubated for 15 min – 45 min at 37 °C with 5 % CO_2. In previous work, the seeding time was determined with capture efficiencies of over 80 % for Pf4cre megakaryocytes (**Suppl. Figure 4B**). The channels were then perfused under a flow of 300 µm/s and the

megakaryocyte behavior was monitored in real-time, for 1 min, using a Leica DMI8 microscope (x20) equipped with a CMOS Camera (Hamamatsu ORCA fusion). Megakaryocyte capture yield was measured by quantifying the number of adherent megakaryocytes before and after flow induction (expressed as a percentage) on an average of 20 stage positions (n= 50 megakaryocytes analyzed/test). The results are an average of three independent experiments, the values were expressed as a mean ± sem.

Bone marrow explants

Preparation of bone marrow explants was performed as described in Guinard et al., 2021 to investigate proplatelet formation. For investigating megakaryocyte emigration, bone marrows were flushed from femurs of *Pf4cre* and*Itgb1*$^{-/-}$/*Itgb3*$^{-/-}$; Lamα4$^{+/+}$ and Lamα4$^{-/-}$; as well as from DMSO- and B+I-treated mice and ten 0.5 mm-thick sections were placed in an incubation chamber. Megakaryocytes at the periphery of the explants were counted under an inverted phase contrast microscope coupled to a video camera (DMI8 Leica microscope, 40x objective). A motorized multiposition stage (in *x*, *y*, *z*) was used, and an average of 100 stages positions showing megakaryocytes was followed. Results are expressed as the number of total emigrating megakaryocytes at the indicated time points. In each case, a minimum of six independent experiments were performed. Mice from each genotype were analyzed and image acquisitions were performed in a blinded manner.

Effects of MMP inhibition

Batimastat plus ilomastat treatment was tested for their potential impact on the ECM in the microenvironment of the megakaryocyte vascular niche. Mice were treated daily with a protease inhibitor cocktail (Batimastat at 30 mg/kg + Ilomastat at 50 mg/kg) or vehicle (DMSO) for 7 consecutive days (Gui et al., 2018; Pielecka-Fortuna et al., 2015). The platelet count was monitored every two days. On the eighth day, the mice were sacrificed, and their bone marrow was collected for analysis of ECM organization and megakaryocyte behavior, as explained in the 3D confocal analysis on bone marrow vibratome sections.

Gelatin degradation assay

Coverslips were coated with Oregon green gelatin, and fixed with 0.5% glutaraldehyde for 20 min at RT. After washing three times with PBS, cells were seeded on coated coverslips and incubated for 6 h before fixation and staining.

Statistics

All values are reported as the mean ± sem. n= number of megakaryocytes studied. Statistical analyses were performed with PrismGraphpad software (La Jolla, CA, USA). For group comparison, data were tested for Gaussian distribution. Then, a Student t-test (Gaussian) or Mann-Whitney U test (non-Gaussian) were used to compare individual groups; multiple groups were compared by one-way ANOVA followed by Bonferroni post-test or by a non-parametric Kruskal-Wallis test, with a threshold of significance of 5%. P-values <0.05 were considered statistically significant. *P<0.05; **P<0.01; ***P<0.001.

Acknowledgements

We wish to thank Ketty Knez-Hippert, Josiane Weber, Clarisse Mouriaux, Sylvie Moog and Patricia Laeuffer (EFS-GEST) for excellent expert technical assistance. This work was supported by ARMESA (Association de Recherche et Développement en Médecine et Santé Publique) and by ANR Grant MegaPod (ANR-22-CE14-0029). The authors thank Pr. B. Nieswandt for providing GPVI knock-out mice.

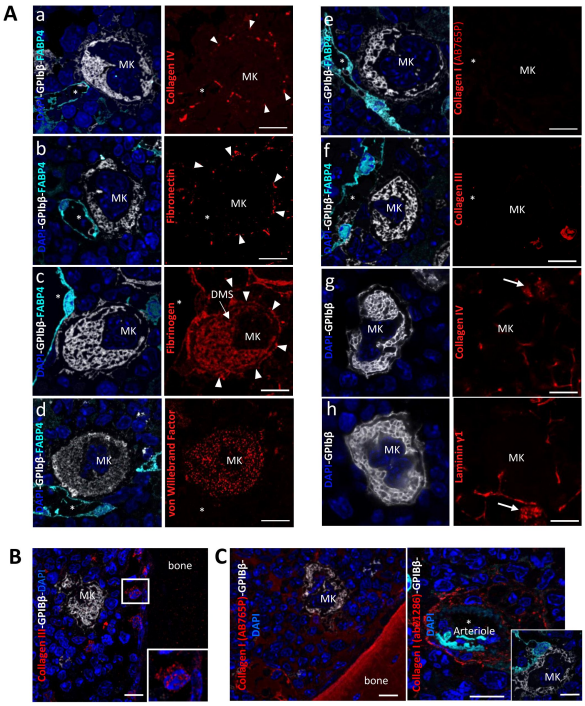

Supplemental Figure 1

Molecular cartography of the ECM around megakaryocytes.

(A) Immunofluorescence 2D analysis of ECM proteins. Collagen IV (a and g), laminin γ1 (h), fibronectin (b), fibrinogen (c), von Willebrand factor (d), and collagen I /III (e-f) around sinusoid-associated megakaryocytes. Bone marrow immunostained for GPIbβ(white), FABP4 (cyan), and DAPI (blue).
(B) Positive immunostaining of small stromal cells near the bone with the antibody against collagen III.
(C) Positive immunostaining of the bone and arterioles using two antibody against collagen I (AB765P and ab21286, respectively). Note that the megakaryocytes are not immunostained.
(D-E) Direct connections between the basement membrane and the ECM cage
D. Maximal projection showing the interface between the basement membrane (red), the sinusoid (blue) and megakaryocyte (white). The next image is a 3D reconstruction of this area.
E. Maximum projection of 3D laminin Y1 fibers linked to the basement membrane. The arrowheads indicate the connextion between the basement membrane and the cage.
(F-H) The spatial distribution of the ECM cage is highly restrictive to the sinusoid-associated megakaryocytes
F. Maximal projection of a large field of the 3D laminin Y1 organization. Megakaryocytes in contact with sinusoids (sMK) have a cage, while megakaryocytes in the parenchyma (pMK) were surrounded by sparse interstitial laminin Y1. Bone marrow immunostained for GPIbβ(white) and laminin Y1 (red).
G. Quantification of the number of megakaryocytes displaying the typical 3D cage as a function of cell association with sinusoids. Megakaryocytes with an ECM cage (grey bars) and without a cage (hatched bars) were counted (three complete 3D stacks from independent mice, 126 megakaryocytes counted in total as indicated in the bars, **P<0.01 Mann-Whitney).
H. Quantification of the pMK relative to the total MK population. Megakaryocytes in the stroma and in contact with sinusoids were counted on three complete 3D stacks from independent mice, ***P<0.0001, unpaired t-test). OK
(I-J) Correlation with the maturation stages of megakaryocytes.
I. Maximal projections of megakaryocytes are shown. Bone marrow immunostained for GPIbβ(white) and laminin Y1 (red).
J. Quantification of laminin γ1 immunostaining on megakaryocytes. Quantification per cell shows the presence of a 3D ECM cage at all stages of maturation (2-3 independent experiments, 14<n<22 as indicated in the bars, *P<0,05 Mann-Whitney). Quantification on megakaryocytes extending proplatelets and residual megakaryocytes was not possible due to sample size limitations.
(K) Distribution of fibronectin and fibrinogen around sinusoid-associated megakaryocytes. Maximal projection 3D images showing the absence of ECM connections with the basement membrane for fibronectin (magenta) and fibrinogen (yellow). Sinusoid endothelial cells were visualized with anti-FABP4 (cyan) and megakaryocytes were identified with anti-GPIbβ (white). Arrowheads, peri-MK staining; Arrow, staining in adjacent small cells in (Ag-h); bm, basement membrane; MK, megakaryocyte; DMS, demarcation membrane system; PPT, proplatelet; *, vascular lumen; Bar, 10 μm.

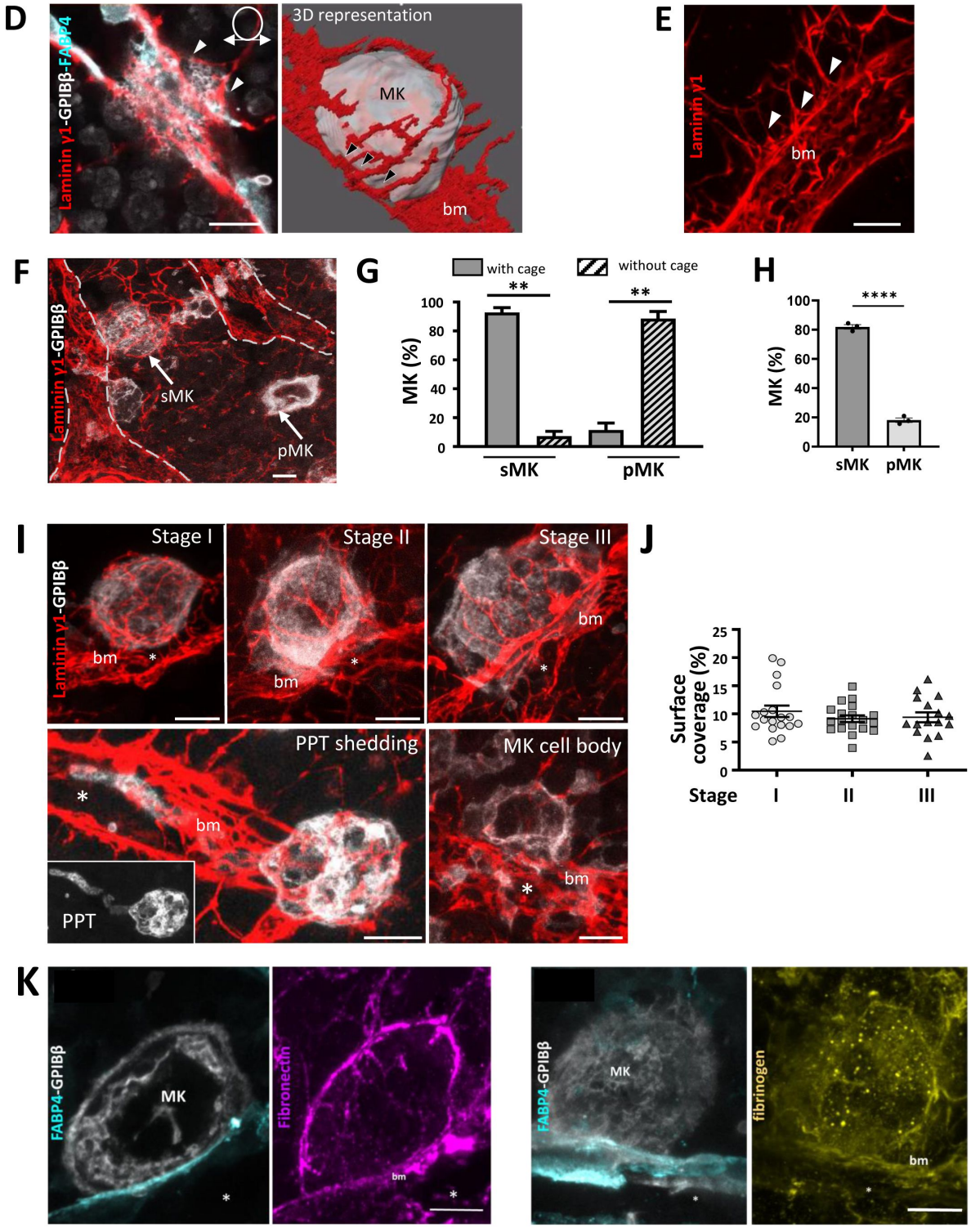

Supplemental Figure 1 (continued)

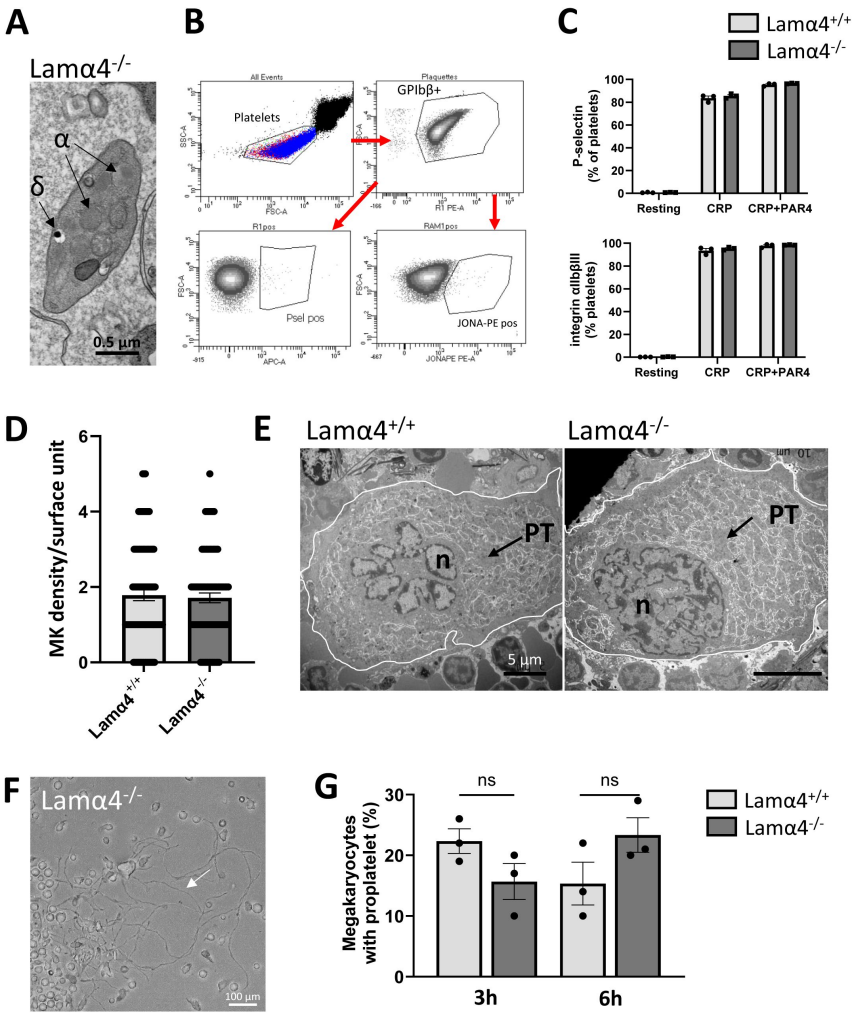

Supplementary Figure 2

Characterization of Lamα4$^{-/-}$ platelets and megakaryocytes

(A-C) Lamα4$^{-/-}$ platelet morphology and functions.
A. Normal size, discoid shape and ultrastructure of Lamα4$^{-/-}$ platelets. Bar: 0.5 µm.
B. Gating strategy for platelet function analysis. Flow cytometry was used to analyse the functions of Lamα4-/- platelets. Following activation with collagen-related peptide (CRP)(40 µg/ml) or CRP + TRAP (4 mM), the expression of P-selectin (CD62P, a marker of α-granule secretion) and P-selectin (JON-A PE, a marker of integrin αIIbβ3 activation) was analyzed.
C. Quantification of the percentage of positive platelets, Bars are the mean ± standard error of the mean (SEM) of 3 to 6 independent experiments. The results were statistically compared to those of control platelets (*P < 0.05; **P < 0.01; ***P < 0.001).
(D-E) Megakaryopoiesis in Lamα4$^{-/-}$ mice.
D. Quantification of the bone marrow megakaryocytes observed by electron microscopy, per surface unit (s.u., 12,945 µm^2). ns, p=0,7177 unpaired t test.
E. Representative TEM images of Lamα4$^{+/+}$ and Lamα4$^{-/-}$ megakaryocytes. Bars, 5 µm.
(F-G) Ex vivo capacity of of Lamα4$^{-/-}$ megakaryocytes to form proplatelets.
F. Representative image showing proplatelets forming-Lamα4$^{-/-}$ megakaryocytes in fresh bone marrow explants. Arrowhead pointes to proplatelets. Scale Bar, 100 µm.
G. Quantification of the percentage of Lamα4$^{+/+}$ and Lamα4$^{-/-}$ megakaryocytes extending proplatelets following 3h and 6h h. Bars represent the mean ± SEM of three independent experiments (107<n<113 for Lamα4$^{+/+}$ and Lamα4$^{-/-}$, ns p>0.1, unpaired t-test).
α, alpha granules, δ, dense granules, PT, platelet territories, bm, basement membrane, MK, megakaryocyte*, sinusoid lumen. Bars, 10 µm.

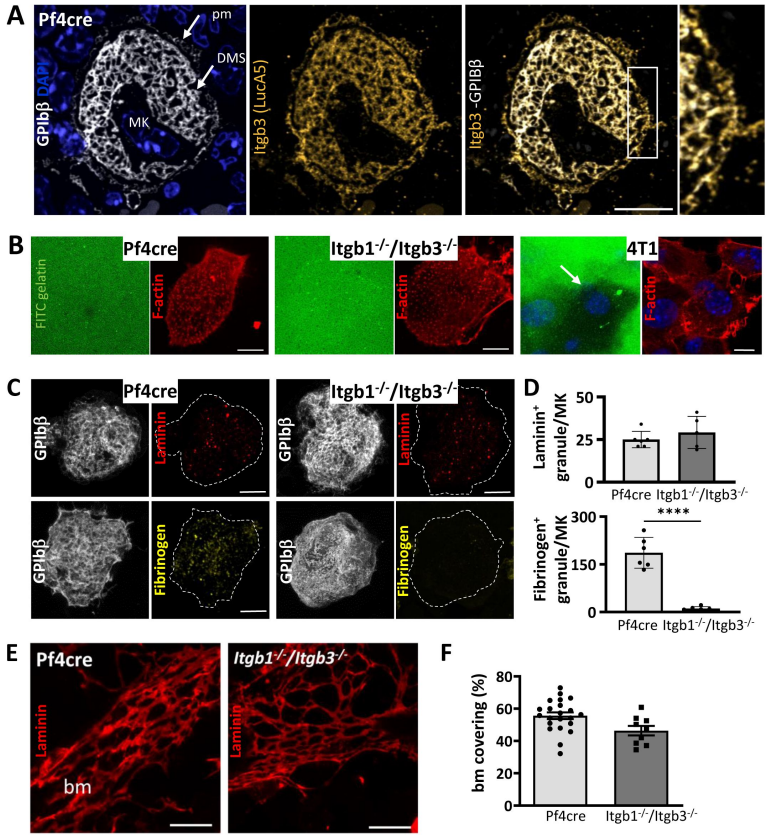

Supplementary Figure 3

Integrins control the structural properties of the ECM cages around megakaryocytes

(**A**) Representative 2D images of sinusoid-associated megakaryocyte immunostained for β3 integrin (LucA5 in yellow). Right panel: the boxed area is shown at a higher magnification.
(B) Itgb1$^{-/-}$/Itgb3$^{-/-}$ megakaryocytes did not display enhanced degradation of gelatin matrix. Freshly isolated megakaryocytes from Pf4cre or Itgb1$^{-/-}$/Itgb3$^{-/-}$ bone marrow were deposited on a fluorescent gelatin matrix (green) for 3h and labeled with phalloidin (adhesive structures in red). ECM degradation was virtually absent in Pf4cre and Itgb1$^{-/-}$/Itgb3$^{-/-}$ megakaryocytes. Tumoral 4T1 cells, which trigger large dark digested areas (arrow), were used as a positive control.
(C-D) Laminin is present in similar amounts in Itgb1$^{-/-}$/Itgb3$^{-/-}$ and Pf4cre megakaryocytes.
C. Maximal projection 3D images illustrating the presence or not of granules containing laminin (in red) and fibrinogen (in yellow, as negative control) in megakaryocytes (in white) from freshly isolated Pf4cre and Itgb1$^{-/-}$/Itgb3$^{-/-}$ megakaryocytes. The dotted lines delineated megakaryocytes.
D. Quantification of the number of granules per megakaryocyte (5<MK<6, ****P>0.001, t-test).
(E-F) Normal laminin deposition in the sinusoid basement membrane in Itgb1$^{-/-}$/Itgb3$^{-/-}$
E. Representative 3D images of basement membrane immunostained for laminin Y1 (red) (from one out of three independent IF experiments).
F. Quantification of fluorescence intensity of laminin per basement membrane surface (expressed as a percentage).
(G-H) Fibronectin and fibrinogen failed to form a ECM cage around Pf4cre and Itgb1$^{-/-}$/Itgb3$^{-/-}$ megakaryocytes
G. Decrease in the expression of fibrillar fibronectin around Itgb1$^{-/-}$/Itgb3$^{-/-}$ megakaryocytes.
H. Mislocalization of fibrinogen in Itgb1$^{-/-}$/Itgb3$^{-/-}$ megakaryocytes.
Top panels. 2D immunofluorescence of Pf4cre and Itgb1$^{-/-}$/Itgb3$^{-/-}$ bone marrow cryosections using anti-fibronectin (magenta) and anti-fibrinogen (green) antibodies.
Lower panels ImmunogoldEM images showing the fibronectin and fibrinogen stainings with 10 nm gold particles. Without integrins, megakaryocytes are unable to effectively remodel fibronectin into fibers. Fibrinogen staining is located in the α granules of Pf4cre megakaryocytes and retained in the extracellular DMS space of Itgb1$^{-/-}$/Itgb3$^{-/-}$ megakaryocytes.
α, alpha granules; arrowheads, peri-MK staining; bm, basement membrane; MK, megakaryocyte; pm, plasma membrane; *, sinusoid lumen; Bar, 10 µm.

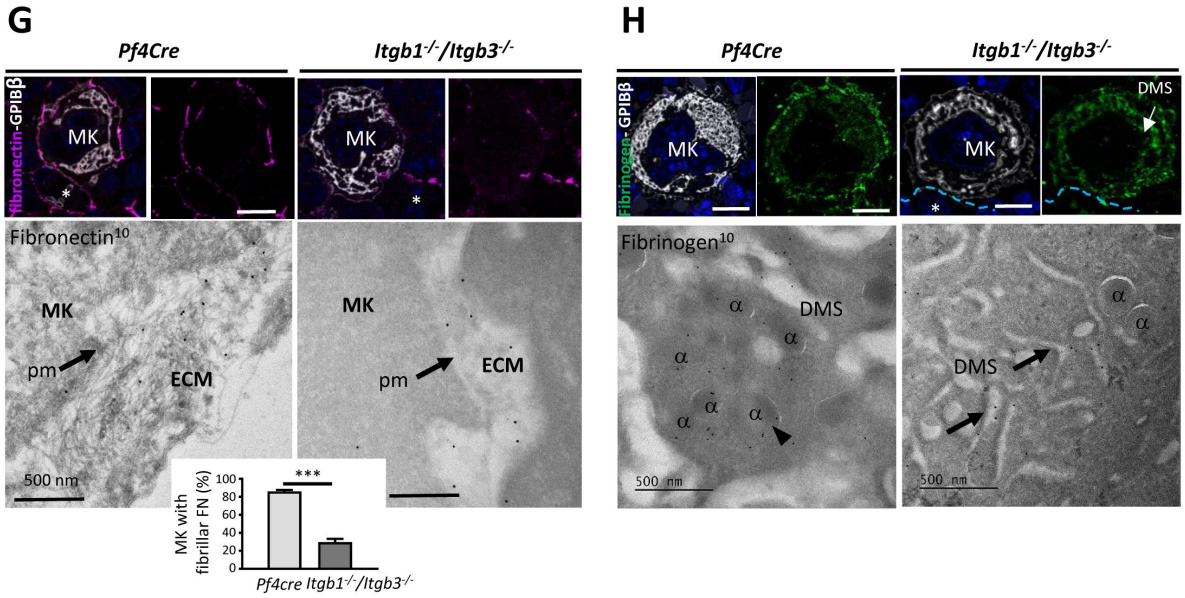

Supplementary Figure 3 (continued)

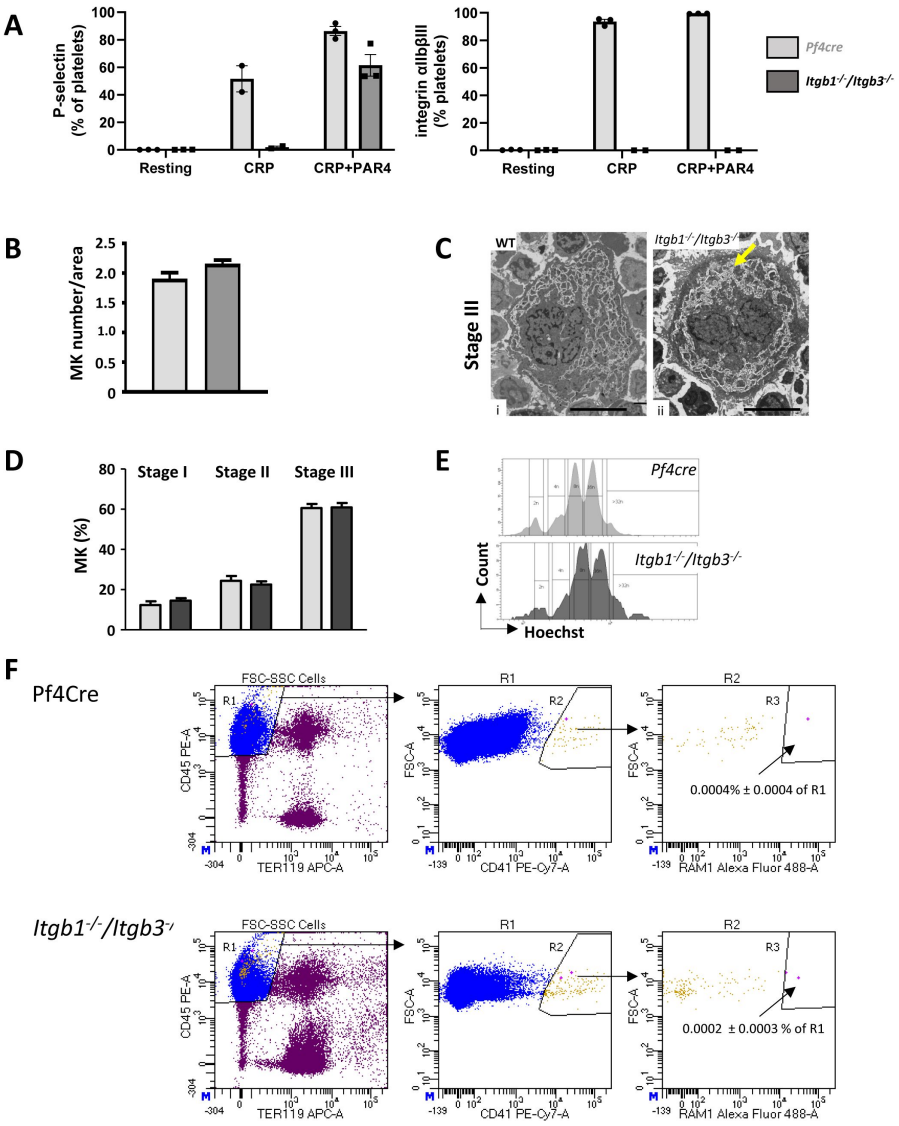

Supplemental Figure 4

Characterization of *Itgb1*$^{-/-}$/*Itgb3*$^{-/-}$ platelets and megakaryocytes

(A) *Itgb1*$^{-/-}$/*Itgb3*$^{-/-}$ platelet functional properties assessed by flow cytometry.
The gating strategy was similar to that in **Supplemental Figure 2B**. Bar graphs showing that activated Itgb1$^{-/-}$/Itgb3$^{-/-}$ platelets expressed P-selectin but not JON-A PE. This confirmed their deficiency in integrin β3 (n=3 mice per genotype).
(B-E) Megakaryocyte density, maturation stages and ploidy were normal in *Itgb1*$^{-/-}$/*Itgb3*$^{-/-}$ bone marrow
B. Quantification of the total number of megakaryocyte, observed by electron microscopy (from 6-7 independent experiments, 120<n<153 as indicated in the bars).
C. Representative TEM images of stage III megakaryocytes. (i) The DMS is well-defined with the presence of cytoplasmic territories in control mice. (ii) In *Itgb1*$^{-/-}$/*Itgb3*$^{-/-}$ mice, the DMS accumulates in packets without marking territories (yellow arrow). Bars: 5 µm.
D. Classification of the megakaryocytes according to their maturation stage (from 3-5 independent experiments, 99<n<544).
E. Representative ploidy histograms of *Pf4cre* and *Itgb1*$^{-/-}$/*Itgb3*$^{-/-}$ megakaryocyte (one out of three independent experiments).
(F) Intact megakaryocytes were undetectable in the blood of Itgb1$^{-/-}$/Itgb3$^{-/-}$ mice.
Gating strategy for megakaryocyte identification: CD45+TER119-cells were selected from events with high FSC and SSC parameter (excluding platelets), CD41bright and CD42c bright events are megakaryocytes. The gate positions were determined based on FMO controls and biological positive controls (mouse bone marrow MK enriched cell suspension and whole blood supplemented with MK enriched cell population) (data not shown). Representative plots from 3 separate acquisitions on *Pf4cre* and *Itgb1*$^{-/-}$/*Itgb3*$^{-/-}$ mice.

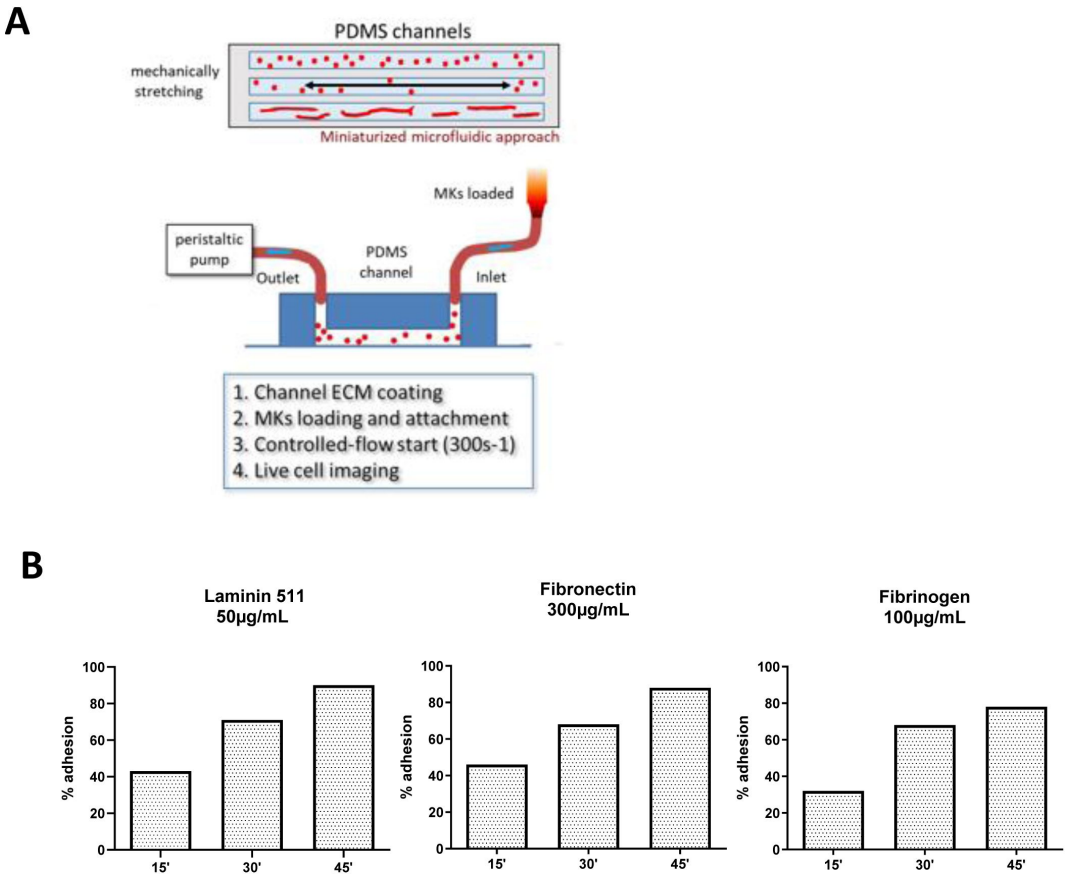

Supplement. Figure 5

Adhesive properties of *Itgb1*$^{-/-}$/*Itgb3*$^{-/-}$ megakaryocytes

(A) Schematic representation of the experimental microfluidic equipment.
(B) Determination of the seeding time with capture efficiencies of over 80 % for *Pf4cre* megakaryocytes on laminin-, fibronectin- or fibrinogen-coated chambers.

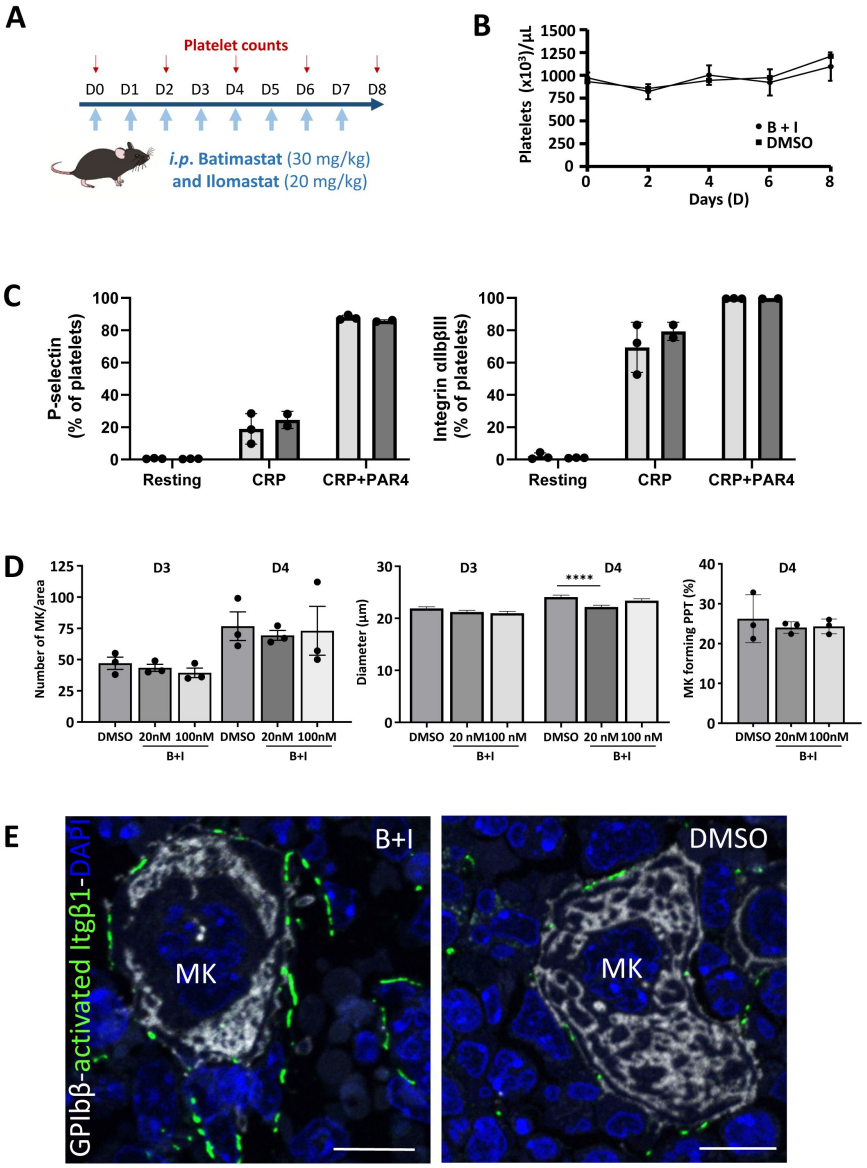

Supplementary Figure 6

Proteolysis inhibition do not affect platelet count and *in vitro* megakaryocyte maturation.

(A) Experimental setup. A combination of batimastat (30 mg/kg) and ilomastat (20 mg/kg) (B + I) or vehicle (DMSO) was injected daily for 7 days.
(B-C) *In vivo* MMP inhibition is not impact platelet count and function.
B. Platelet counts were similar in both groups.
C. Flow cytometry shows normal P-selectin and JON-A PE expression following activation with collagen-related peptide (CRP) (40 µg/ml) or CRP + TRAP (4 mM). Bars graphs represent the percentage of positive platelets, mean ± standard error of the mean (SEM). The results were statistically compared to those of control platelets (ns, multiple unpaired t tests).
(D) *In vitro* studies demonstrate that batimastat and ilomastat have no significant direct effect on cultured megakaryocytes. This is evident from their lack of impact on : 1) proliferation (as expressed by the number of megakaryocytes (MKs) per unit), 2) maturation (as expressed by MK size in µm); 3) the ability to extend proplatelets (as expressed by the percentage of MKs that extend proplatelets). Bar graphs illustrate the impact of two MMP inhibitor doses on days 3 and 4 of the culture process, displaying the mean and standard error of the mean (SEM).
(E) Representative 2D images of bone marrow cryosections demonstrating an increase staining of activated β1 integrin (9EG7 in green) around megakaryocytes in bone marrow treated with B + I in comparison to that treated with DMSO.
*, lumen of the sinusoid; D, day; MK, megakaryocyte; Bars: 10 µm.

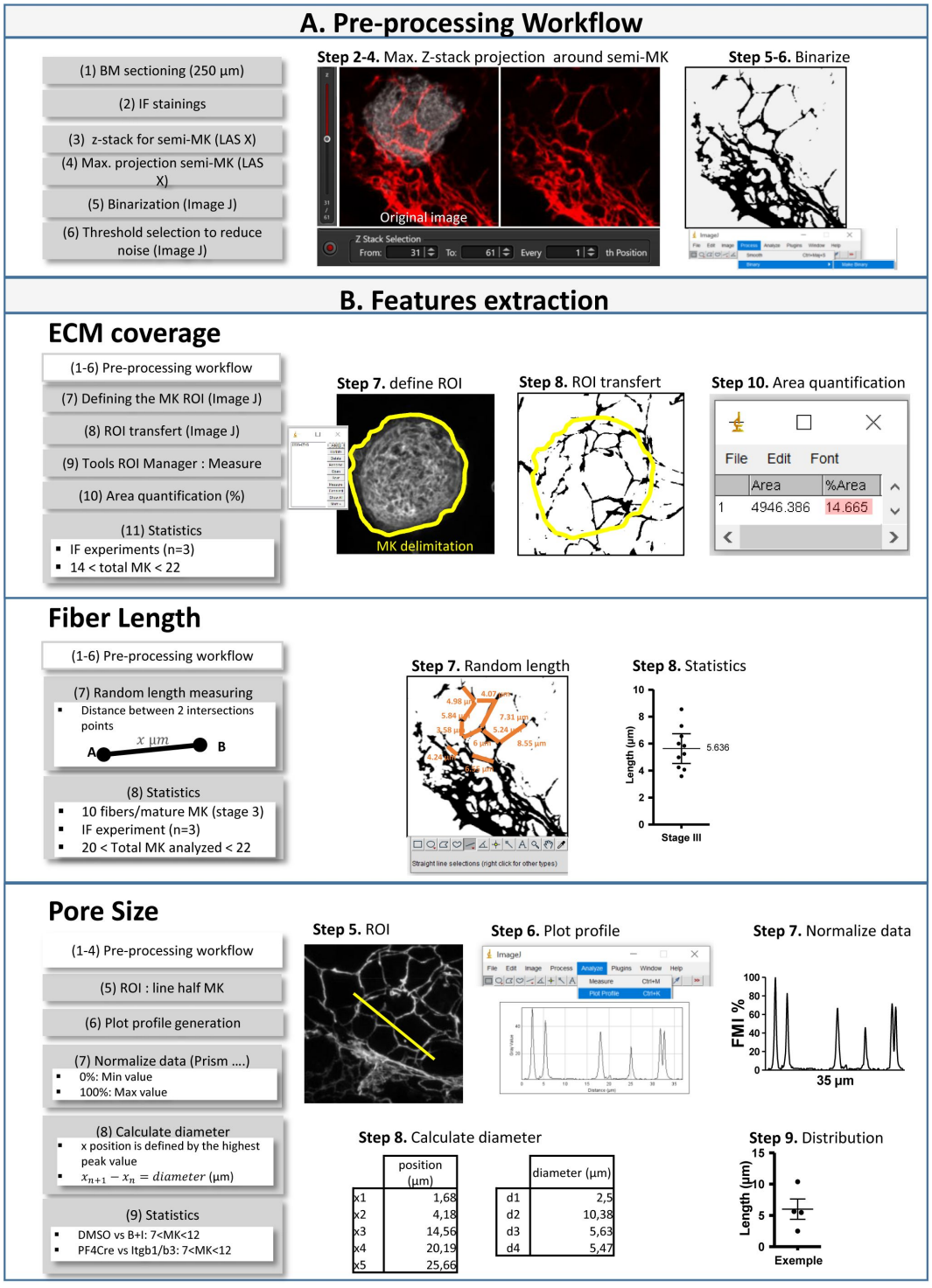

Supplementary Figure 7.

Image data flow graph

Additional information

Contributions

C.M and C.S performed experiments, analyzed data, and contributed to the writing of the revised manuscript; JY.R, F.P, E.J-B, N.O, L.M, A.M., N.B. and A.B performed experiments, analyzed data, and commented on the manuscript; J.G, N.O, C.Q, F.B, and C.L provided vital reagents and commented on the manucript; R.P., O.D, and M.L contributed to the writing of the manuscript; and A.E designed and supervised research, analyzed data, and wrote the manuscript

Additional files

Movie 1

Movie 2

Movie 3

Movie 4

Movie 5

Legend of the movies

Figure source data

References

Abbonante V., Chitalia V., Rosti V., Leiva O., Matsuura S., Balduini A., Ravid K (2017) **Upregulation of lysyl oxidase and adhesion to collagen of human megakaryocytes and platelets in primary myelofibrosis** *Blood* **130**:829–831 https://doi.org/10.1182/blood-2017-04-777417 | Google Scholar

Abbonante V., Di Buduo C. A., Gruppi C., Malara A., Gianelli U., Celesti G., Anselmo A., Laghi L., Vercellino M., Visai L., Iurlo A., Moratti R., Barosi G., Rosti V., Balduini A. (2016) **Thrombopoietin/TGF- β 1 Loop Regulates Megakaryocyte Extracellular Matrix Component Synthesis** *Stem Cells* **34**:1123–1133 https://doi.org/10.1002/stem.2285 | Google Scholar

Abbonante V., Karkempetzaki A. I., Leon C., Krishnan A., Huang N., Di Buduo C. A., Cattaneo D., Ward C. M., Matsuura S., Guinard I., Weber J., De Acutis A., Vozzi G., Iurlo A., Ravid K., Balduini A. (2024) **Newly identified roles for PIEZO1 mechanosensor in controlling normal megakaryocyte development and in primary myelofibrosis** *American Journal of Hematology* **99**:336–349 https://doi.org/10.1002/ajh.27184 | Google Scholar

Aguilar A., Pertuy F., Eckly A., Strassel C., Collin D., Gachet C., Lanza F., Léon C (2016) **Importance of environmental stiffness for megakaryocyte differentiation and proplatelet formation** *Blood* **128**:2022–2032 https://doi.org/10.1182/blood-2016-02-699959 | Google Scholar

Attieh Y., Clark A. G., Grass C., Richon S., Pocard M., Mariani P., Elkhatib N., Betz T., Gurchenkov B., Vignjevic D. M (2017) **Cancer-associated fibroblasts lead tumor invasion through integrin-β3–dependent fibronectin assembly** *Journal of Cell Biology* **216**:3509–3520 https://doi.org/10.1083/jcb.201702033 | Google Scholar

Avecilla S. T., Hattori K., Heissig B., Tejada R., Liao F., Shido K., Jin D. K., Dias S., Zhang F., Hartman T. E., Hackett N. R., Crystal R. G., Witte L., Hicklin D. J., Bohlen P., Eaton D., Lyden D., De Sauvage F., Rafii S. (2004) **Chemokine-mediated interaction of hematopoietic progenitors with the bone marrow vascular niche is required for thrombopoiesis** *Nature Medicine* **10**:64–71 https://doi.org/10.1038/nm973 | Google Scholar

Balduini A., Pallotta I., Malara A., Lova P., Pecci A., Viarengo G., Balduini C. L., Torti M (2008) **Adhesive receptors, extracellular proteins and myosin IIA orchestrate proplatelet formation by human megakaryocytes** *Journal of Thrombosis and Haemostasis: JTH* **6**:1900–1907 https://doi.org/10.1111/j.1538-7836.2008.03132.x | Google Scholar

Barriga E. H., Franze K., Charras G., Mayor R (2018) **Tissue stiffening coordinates morphogenesis by triggering collective cell migration in vivo** *Nature* **554**:523–527 https://doi.org/10.1038/nature25742 | Google Scholar

Bender M., Hagedorn I., Nieswandt B (2011) **Genetic and antibody-induced glycoprotein VI deficiency equally protects mice from mechanically and FeCl3-induced thrombosis** *Journal of Thrombosis and Haemostasis* **9**:1423–1426 https://doi.org/10.1111/j.1538-7836.2011.04328.x | Google Scholar

Bornert A., Boscher J., Pertuy F., Eckly A., Stegner D., Strassel C., Gachet C., Lanza F., Léon C (2021) **Cytoskeletal-based mechanisms differently regulate in vivo and in vitro proplatelet formation** *Haematologica* **106**:Article 5 https://doi.org/10.3324/haematol.2019.239111 | Google Scholar

Boscher J., Guinard I., Eckly A., Lanza F., Léon C. (2020) **Blood platelet formation at a glance** *Journal of Cell Science* **133**:jcs244731 https://doi.org/10.1242/jcs.244731 | Google Scholar

Cai H., Kondo M., Sandhow L., Xiao P., Johansson A.-S., Sasaki T., Zawacka-Pankau J., Tryggvason K., Ungerstedt J., Walfridsson J., Ekblom M., Qian H (2022) **Critical role of Lama4 for hematopoiesis regeneration and acute myeloid leukemia progression** *Blood* **139**:3040–3057 https://doi.org/10.1182/blood.2021011510 | Google Scholar

De Mets R., Wang I., Balland M., Oddou C., Moreau P., Fourcade B., Albiges-Rizo C., Delon A., Destaing O. (2019) **Cellular tension encodes local Src-dependent differential β1 and β3 integrin mobility** *Molecular Biology of the Cell* **30**:181–190 https://doi.org/10.1091/mbc.E18-04-0253 | Google Scholar

Dolega M. E., Monnier S., Brunel B., Joanny J.-F., Recho P., Cappello G (2021) **Extracellular matrix in multicellular aggregates acts as a pressure sensor controlling cell proliferation and motility** *eLife* **10**:e63258 https://doi.org/10.7554/eLife.63258 | Google Scholar

Eliades A., Papadantonakis N., Bhupatiraju A., Burridge K. A., Johnston-Cox H. A., Migliaccio A. R., Crispino J. D., Lucero H. A., Trackman P. C., Ravid K (2011) **Control of Megakaryocyte Expansion and Bone Marrow Fibrosis by Lysyl Oxidase** *Journal of Biological Chemistry* **286**:27630–27638 https://doi.org/10.1074/jbc.M111.243113 | Google Scholar

Frydman G. H., Ellett F., Jorgensen J., Marand A. L., Zukerberg L., Selig M. K., Tessier S. N., Wong K. H. K., Olaleye D., Vanderburg C. R., Fox J. G., Tompkins R. G., Irimia D (2023) **Megakaryocytes respond during sepsis and display innate immune cell behaviors** *Frontiers in Immunology* **14**:1083339 https://doi.org/10.3389/fimmu.2023.1083339 | Google Scholar

Gaertner F., et al (2024) **Plasmacytoid dendritic cells control homeostasis of megakaryopoiesis** *Nature* **631**:645–653 https://doi.org/10.1038/s41586-024-07671-y | Google Scholar

Gelon L., Fromont L., Lefrançais E (2022) **Occurrence and role of lung megakaryocytes in infection and inflammation** *Frontiers in Immunology* **13** https://www.frontiersin.org/articles/10.3389/fimmu.2022.1029223 | Google Scholar

Gianelli U., Thiele J., Orazi A., Gangat N., Vannucchi A. M., Tefferi A., Kvasnicka H. M (2023) **International Consensus Classification of myeloid and lymphoid neoplasms : Myeloproliferative neoplasms** *Virchows Archiv* **482**:53–68 https://doi.org/10.1007/s00428-022-03480-8 | Google Scholar

Giannini S., Lee-Sundlov M. M., Rivadeneyra L., Di Buduo C. A., Burns R., Lau J. T., Falet H., Balduini A., Hoffmeister K. M. (2020) **β4GALT1 controls β1 integrin function to govern thrombopoiesis and hematopoietic stem cell homeostasis** *Nature Communications* **11**:356 https://doi.org/10.1038/s41467-019-14178-y | Google Scholar

Gui P., Ben-Neji M., Belozertseva E., Dalenc F., Franchet C., Gilhodes J., Labrousse A., Bellard E., Golzio M., Poincloux R., Maridonneau-Parini I., Le Cabec V. (2018) **The Protease-Dependent Mesenchymal Migration of Tumor-Associated Macrophages as a Target in Cancer**

Immunotherapy *Cancer Immunology Research* **6**:1337–1351 https://doi.org/10.1158/2326-6066.CIR-17-0746 | Google Scholar

Guinard I., Nguyen T., Brassard-Jollive N., Weber J., Ruch L., Reininger L., Brouard N., Eckly A., Collin D., Lanza F., Léon C (2023) **Matrix stiffness controls megakaryocyte adhesion, fibronectin fibrillogenesis, and proplatelet formation through Itgβ3** *Blood Advances* **7**:4003–4018 https://doi.org/10.1182/bloodadvances.2022008680 | Google Scholar

Hamada T., Möhle R., Hesselgesser J., Hoxie J., Nachman R. L., Moore M. A. S., Rafii S (1998) **Transendothelial Migration of Megakaryocytes in Response to Stromal Cell-derived Factor 1 (SDF-1) Enhances Platelet Formation** *Journal of Experimental Medicine* **188**:539–548 https://doi.org/10.1084/jem.188.3.539 | Google Scholar

Handagama P. J., George J. N., Shuman M. A., McEver R. P., Bainton D. F (1987) **Incorporation of a circulating protein into megakaryocyte and platelet granules** *Proceedings of the National Academy of Sciences* **84**:861–865 https://doi.org/10.1073/pnas.84.3.861 | Google Scholar

Janus-Bell E., Receveur N., Mercier L., Mouriaux C., Magnenat S., Reiser J., Lanza F., Hechler B., Ho-Tin-Noé B., Mangin P. H (2024) **Cooperation Between Platelet β1 and β3 Integrins in the Arrest of Bleeding Under Inflammatory Conditions in Mice—Brief Report** *Arteriosclerosis, Thrombosis & Vascular Biology* **44**:2213–2222 https://doi.org/10.1161/ATVBAHA.124.321104 | Google Scholar

Kyumurkov A., Bouin A.-P., Boissan M., Manet S., Baschieri F., Proponnet-Guerault M., Balland M., Destaing O., Régent-Kloeckner M., Calmel C., Nicolas A., Waharte F., Chavrier P., Montagnac G., Planus E., Albiges-Rizo C (2023) **Force tuning through regulation of clathrin-dependent integrin endocytosis** *Journal of Cell Biology* **222**:e202004025 https://doi.org/10.1083/jcb.202004025 | Google Scholar

Larsen M., Artym V. V., Green J. A., Yamada K. M (2006) **The matrix reorganized : Extracellular matrix remodeling and integrin signaling** *Current Opinion in Cell Biology* **18**:463–471 https://doi.org/10.1016/j.ceb.2006.08.009 | Google Scholar

Larson M. K., Watson S. P (2006) **Regulation of proplatelet formation and platelet release by integrin αIIbβ3** *Blood* **108**:1509–1514 https://doi.org/10.1182/blood-2005-11-011957 | Google Scholar

Leiva O., Leon C., Ng S. K., Mangin P., Gachet C., Ravid K (2018) **The Role of Extracellular Matrix Stiffness in Megakaryocyte Development and Function** *American journal of hematology* **93**:430–441 https://doi.org/10.1002/ajh.25008 | Google Scholar

Lemmon C. A., Chen C. S., Romer L. H (2009) **Cell Traction Forces Direct Fibronectin Matrix Assembly** *Biophysical Journal* **96**:729–738 https://doi.org/10.1016/j.bpj.2008.10.009 | Google Scholar

Lepage A., Leboeuf M., Cazenave J. P., de la Salle C., Lanza F., Uzan G. (2000) **The alpha(IIb)beta(3) integrin and GPIb-V-IX complex identify distinct stages in the maturation of CD34(+) cord blood cells to megakaryocytes** *Blood* **96**:4169 Google Scholar

Lichtman M. A., Chamberlain J. K., Simon W., Santillo P. A (1978) **Parasinusoidal location of megakaryocytes in marrow : A determinant of platelet release** *American Journal of Hematology* **4**:303–312 https://doi.org/10.1002/ajh.2830040402 | Google Scholar

Malara A., Currao M., Gruppi C., Celesti G., Viarengo G., Buracchi C., Laghi L., Kaplan D. L., Balduini A (2014) **Megakaryocytes contribute to the bone marrow-matrix environment by expressing fibronectin, type IV collagen and laminin** *Stem cells* **32**:926–937 https://doi.org/10.1002/stem.1626 | Google Scholar

Malara A., Gruppi C., Abbonante V., Cattaneo D., De Marco L., Massa M., Iurlo A., Gianelli U., Balduini C. L., Tira M. E., Muro A. F., Chauhan A. K., Rosti V., Barosi G., Balduini A. (2019) **EDA fibronectin–TLR4 axis sustains megakaryocyte expansion and inflammation in bone marrow fibrosis** *Journal of Experimental Medicine* **216**:587–604 https://doi.org/10.1084/jem.20181074 | Google Scholar

Malara A., Ligi D., Di Buduo C. A., Mannello F., Balduini A. (2018) **Sub-Cellular Localization of Metalloproteinases in Megakaryocytes** *Cells* **7** https://doi.org/10.3390/cells7070080 | Google Scholar

Matsuura S., Thompson C. R., Ng S. K., Ward C. M., Karagianni A., Mazzeo C., Malara A., Balduini A., Ravid K (2020) **Adhesion to fibronectin via α5β1 integrin supports expansion of the megakaryocyte lineage in primary myelofibrosis** *Blood* **135**:2286–2291 https://doi.org/10.1182/blood.2019004230 | Google Scholar

Maurer E., Schaff M., Receveur N., Bourdon C., Mercier L., Nieswandt B., Dubois C., Jandrot-Perrus M., Goetz J. G., Lanza F., Gachet C., Mangin P. H (2015) **Fibrillar cellular fibronectin supports efficient platelet aggregation and procoagulant activity** *Thrombosis and Haemostasis* **114**:1175–1188 https://doi.org/10.1160/TH14-11-0958 | Google Scholar

Morgan E. A., Schneider J. G., Baroni T. E., Uluçkan O., Heller E., Hurchla M. A., Deng H., Floyd D., Berdy A., Prior J. L., Piwnica-Worms D., Teitelbaum S. L., Ross F. P., Weilbaecher K. N. (2010) **Dissection of platelet and myeloid cell defects by conditional targeting of the β3-integrin subunit** *The FASEB Journal* **24**:1117–1127 https://doi.org/10.1096/fj.09-138420 | Google Scholar

Oprescu A., Michel D., Antkowiak A., Vega E., Viaud J., Courtneidge S. A., Eckly A., De La Salle H., Chicanne G., Léon C., Payrastre B., Gaits-Iacovoni F. (2022) **Megakaryocytes form linear podosomes devoid of digestive properties to remodel medullar matrix** *Scientific Reports* **12**:6255 https://doi.org/10.1038/s41598-022-10215-x | Google Scholar

Osmani N., Follain G., Gensbittel V., García-León M. J., Harlepp S., Goetz J. G (2021) **Probing Intravascular Adhesion and Extravasation of Tumor Cells with Microfluidics** *Methods Mol Biol* **2294**:111–132 https://doi.org/10.1007/978-1-0716-1350-4_8 | Google Scholar

Ouzegdouh Y., Capron C., Bauer T., Puymirat E., Diehl J.-L., Martin J. F., Cramer-Bordé E (2018) **The physical and cellular conditions of the human pulmonary circulation enable thrombopoiesis** *Experimental Hematology* **63**:22–27 https://doi.org/10.1016/j.exphem.2018.04.001 | Google Scholar

Petito E., Gresele P (2024) **Immune attack on megakaryocytes in immune thrombocytopenia** *Research and Practice in Thrombosis and Haemostasis* **8**:102345 https://doi.org/10.1016/j.rpth.2024.102345 | Google Scholar

Petrey A. C., Obery D. R., Kessler S. P., Flamion B., De La Motte C. A. (2016) **Hyaluronan Depolymerization by Megakaryocyte Hyaluronidase-2 Is Required for Thrombopoiesis** *The*

American Journal of Pathology **186**:2390–2403 https://doi.org/10.1016/j.ajpath.2016.05.004 | Google Scholar

Pielecka-Fortuna J., Kalogeraki E., Fortuna M. G., Löwel S (2015) **Optimal level activity of matrix metalloproteinases is critical for adult visual plasticity in the healthy and stroke-affected brain** *eLife* **4**:e11290 https://doi.org/10.7554/eLife.11290 | Google Scholar

Piszczatowski R. T., Schwenger E., Sundaravel S., Stein C. M., Liu Y., Stanley P., Verma A., Zheng D., Seidel R. D., Almo S. C., Townley R. A., Bülow H. E., Steidl U (2022) **A glycan-based approach to cell characterization and isolation : Hematopoiesis as a paradigm** *Journal of Experimental Medicine* **219**:e20212552 https://doi.org/10.1084/jem.20212552 | Google Scholar

Potocnik A. J., Brakebusch C., Fässler R (2000) **Fetal and Adult Hematopoietic Stem Cells Require β1 Integrin Function for Colonizing Fetal Liver, Spleen, and Bone Marrow** *Immunity* **12**:653–663 https://doi.org/10.1016/S1074-7613(00)80216-2 | Google Scholar

Puhm F., Laroche A., Boilard E (2023) **Diversity of Megakaryocytes** *Arteriosclerosis, Thrombosis, and Vascular Biology* **43**:2088–2098 https://doi.org/10.1161/ATVBAHA.123.318782 | Google Scholar

Radley J. M., Haller C. J (1983) **Fate of senescent megakaryocytes in the bone marrow** *British Journal of Haematology* **53**:277–287 https://doi.org/10.1111/j.1365-2141.1983.tb02022.x | Google Scholar

Rapkiewicz A. V., Mai X., Carsons S. E., Pittaluga S., Kleiner D. E., Berger J. S., Thomas S., Adler N. M., Charytan D. M., Gasmi B., Hochman J. S., Reynolds H. R (2020) **Megakaryocytes and platelet-fibrin thrombi characterize multi-organ thrombosis at autopsy in COVID-19 : A case series** *eClinicalMedicine* **24**:100434 https://doi.org/10.1016/j.eclinm.2020.100434 | Google Scholar

Sabri S., Jandrot-Perrus M., Bertoglio J., Farndale R. W., Mas V. M.-D., Debili N., Vainchenker W (2004) **Differential regulation of actin stress fiber assembly and proplatelet formation by α2β1 integrin and GPVI in human megakaryocytes** *Blood* **104**:3117–3125 https://doi.org/10.1182/blood-2003-12-4398 | Google Scholar

Sarachakov A., Varlamova A., Svekolkin V., Polyakova M., Valencia I., Unkenholz C., Pannellini T., Galkin I., Ovcharov P., Tabakov D., Postovalova E., Shin N., Sethi I., Bagaev A., Itkin T., Crane G., Kluk M., Geyer J., Inghirami G., Patel S (2023) **Spatial mapping of human hematopoiesis at single-cell resolution reveals aging-associated topographic remodeling** *Blood* **142**:2282–2295 https://doi.org/10.1182/blood.2023021280 | Google Scholar

Saunders J. T., Schwarzbauer J. E (2019) **Fibronectin matrix as a scaffold for procollagen proteinase binding and collagen processing** *Molecular Biology of the Cell* **30**:2218–2226 https://doi.org/10.1091/mbc.E19-03-0140 | Google Scholar

Scandola C., Lanza F., Gachet C., Eckly A (2021) **In Situ Exploration of Murine Megakaryopoiesis using Transmission Electron Microscopy** *Journal of Visualized Experiments* **175**:62494 https://doi.org/10.3791/62494 | Google Scholar

Semeniak D., Faber K., Öftering P., Manukjan G., Schulze H (2019) **Impact of Itga2-Gp6-double collagen receptor deficient mice for bone marrow megakaryocytes and platelets** *PLOS One* **14**:e0216839 https://doi.org/10.1371/journal.pone.0216839 | Google Scholar

Semeniak D., Kulawig R., Stegner D., Meyer I., Schwiebert S., Bösing H., Eckes B., Nieswandt B., Schulze H (2016) **Proplatelet formation is selectively inhibited by collagen type I through Syk-independent GPVI signaling** *Journal of Cell Science* **129**:3473–3484 https://doi.org/10.1242/jcs.187971 | Google Scholar

Stegner D., Angay O., Gorelashvili M. G., Semeniak D., Pinnecker J., Schmithausen P., Meyer I., Friedrich M., Dütting S., Brede C., Beilhack A., Schulze H., Nieswandt B., Heinze K. G. (2017) **Thrombopoiesis is spatially regulated by the bone marrow vasculature** *Nature Communications* **8**:127 https://doi.org/10.1038/s41467-017-00201-7 | Google Scholar

Stone A. P., Nascimento T. F., Barrachina M. N (2022) **The bone marrow niche from the inside out : How megakaryocytes are shaped by and shape hematopoiesis** *Blood* **139**:483–491 https://doi.org/10.1182/blood.2021012827 | Google Scholar

Susek K. H., Korpos E., Huppert J., Wu C., Savelyeva I., Rosenbauer F., Müller-Tidow C., Koschmieder S., Sorokin L (2018) **Bone marrow laminins influence hematopoietic stem and progenitor cell cycling and homing to the bone marrow** *Matrix Biology* **67**:47–62 https://doi.org/10.1016/j.matbio.2018.01.007 | Google Scholar

Villeneuve J., Block A., Le Bousse-Kerdilès M.-C., Lepreux S., Nurden P., Ripoche J., Nurden A. T. (2009) **Tissue inhibitors of matrix metalloproteinases in platelets and megakaryocytes : A novel organization for these secreted proteins** *Experimental Hematology* **37**:849–856 https://doi.org/10.1016/j.exphem.2009.03.009 | Google Scholar

Vögtle T., Sharma S., Mori J., Nagy Z., Semeniak D., Scandola C., Geer M. J., Smith C. W., Lane J., Pollack S., Lassila R., Jouppila A., Barr A. J., Ogg D. J., Howard T. D., McMiken H. J., Warwicker J., Geh C., Rowlinson R., ..., Senis Y. A (2019) **Heparan sulfates are critical regulators of the inhibitory megakaryocyte-platelet receptor G6b-B** *eLife* **8**:e46840 https://doi.org/10.7554/eLife.46840 | Google Scholar

Voisin M.-B., Pröbstl D., Nourshargh S (2010) **Venular Basement Membranes Ubiquitously Express Matrix Protein Low-Expression Regions : Characterization in Multiple Tissues and Remodeling during Inflammation** *The American Journal of Pathology* **176**:482–495 https://doi.org/10.2353/ajpath.2010.090510 | Google Scholar

Wang M., Feng R., Zhang J., Xu L., Feng F., Wang C., Wang Q., Zhu X., He Y., Xue J., Fu H., Lv M., Kong Y., Chang Y., Xu L., Liu K., Huang X., Zhang X (2019) **Dysregulated megakaryocyte distribution associated with nestin+ mesenchymal stem cells in immune thrombocytopenia** *Blood Advances* **3**:1416–1428 https://doi.org/10.1182/bloodadvances.2018026690 | Google Scholar

Winer A., Adams S., Mignatti P (2018) **Matrix Metalloproteinase Inhibitors in Cancer Therapy : Turning Past Failures Into Future Successes** *Molecular Cancer Therapeutics* **17**:1147–1155 https://doi.org/10.1158/1535-7163.MCT-17-0646 | Google Scholar

Yang X., Chitalia S. V., Matsuura S., Ravid K (2022) **Integrins and their role in megakaryocyte development and function** *Experimental Hematology* **106**:31–39 https://doi.org/10.1016/j.exphem.2021.11.007 | Google Scholar

Zeng D. F., Chen F., Wang S., Chen S. L., Xu Y., Shen M. Q., Du C. H., Wang C., Kong P. Y., Cheng T. M., Su Y. P., Wang J. P (2018) **Autoantibody against integrin αvβ3 contributes to**

thrombocytopenia by blocking the migration and adhesion of megakaryocytes *Journal of Thrombosis and Haemostasis* **16**:1843–1856 https://doi.org/10.1111/jth.14214 | Google Scholar

Author information

Claire Masson[≠]
Université de Strasbourg, INSERM, EFS Grand Est, BPPS UMR_S1255, FMTS, Strasbourg, France

[≠]First co-authors ship

Cyril Scandola[≠]
Institut Pasteur, Université Paris Cité, Ultrastructural Bioimaging Unit, Paris, France

[≠]First co-authors ship

Jean-Yves Rinckel
Université de Strasbourg, INSERM, EFS Grand Est, BPPS UMR_S1255, FMTS, Strasbourg, France

Fabienne Proamer
Université de Strasbourg, INSERM, EFS Grand Est, BPPS UMR_S1255, FMTS, Strasbourg, France

Emily Janus-Bell
Université de Strasbourg, INSERM, EFS Grand Est, BPPS UMR_S1255, FMTS, Strasbourg, France

Fareeha Batool
Université de Strasbourg, INSERM, EFS Grand Est, BPPS UMR_S1255, FMTS, Strasbourg, France

Naël Osmani
INSERM UMR_S1109, Tumor Biomechanics Lab, Université de Strasbourg, Fédération de Médecine Translationnelle de Strasbourg (FMTS), Strasbourg, France
ORCID iD: 0000-0003-1195-753X

Jacky G Goetz
INSERM UMR_S1109, Tumor Biomechanics Lab, Université de Strasbourg, Fédération de Médecine Translationnelle de Strasbourg (FMTS), Strasbourg, France
ORCID iD: 0000-0003-2842-8116

Léa Mallo
Université de Strasbourg, INSERM, EFS Grand Est, BPPS UMR_S1255, FMTS, Strasbourg, France

Nathalie Brouard
Université de Strasbourg, INSERM, EFS Grand Est, BPPS UMR_S1255, FMTS, Strasbourg, France

Catherine Léon
Université de Strasbourg, INSERM, EFS Grand Est, BPPS UMR_S1255, FMTS, Strasbourg, France
ORCID iD: 0000-0002-8597-9929

Alicia Bornert
Université de Strasbourg, INSERM, EFS Grand Est, BPPS UMR_S1255, FMTS, Strasbourg, France

Renaud Poincloux
Institut de Pharmacologie et de Biologie Structurale, Université de Toulouse, CNRS, UMR5089, Toulouse, France
ORCID iD: 0000-0003-2884-1744

Olivier Destaing
Institute for Advanced Biosciences, Centre de Recherche Université Grenoble Alpes, Inserm U 1209, CNRS UMR 5309, Grenoble, France

Alma Mansson
Center for Hematology and Regenerative Medicine (HERM), Department of Medicine Hiddinge, Karolinska University Hospital, Karonlinska Institute, Stockholm, Sweden

Hong Qian
Center for Hematology and Regenerative Medicine (HERM), Department of Medicine Hiddinge, Karolinska University Hospital, Karonlinska Institute, Stockholm, Sweden

Maxime Lehmann
Université de Strasbourg, INSERM, EFS Grand Est, BPPS UMR_S1255, FMTS, Strasbourg, France

Anita Eckly
Université de Strasbourg, INSERM, EFS Grand Est, BPPS UMR_S1255, FMTS, Strasbourg, France

For correspondence: anita.michel@efs.sante.fr

Editors

Reviewing Editor
Ambra Pozzi
Vanderbilt University Medical Center, Nashville, United States of America

Senior Editor
Felix Campelo
Universitat Pompeu Fabra, Barcelona, Spain

Reviewer #1 (Public review):

The authors report on a thorough investigation of the interaction of megakaryocytes (MK) with their associated ECM during maturation. They report convincing evidence to support the existence of a dense cage-like pericellular structure containing laminin γ1 and α4 and collagen IV, which interacts with integrins β1 and β3 on MK and serve to fix the perisinusoidal localization of MK and prevent their premature intravasation. As with everything in nature, the authors support a Goldilocks range of MK-ECM interactions - inability to digest the ECM via inhibition of MMPs leads to insufficient MK maturation and development of smaller MK. This important work sheds light into the role of cell-matrix interactions in MK maturation, and suggests that higher-dimensional analyses are necessary to capture the full scope of cellular biology in the context of their microenvironment. The authors have responded appropriately to the majority of my previous comments.

Some remaining points:

In a previous critique, I had suggested that "it is unclear how activation of integrins allows the MK to become "architects for their ECM microenvironment" as the authors posit. A transcriptomic analysis of control and DKO MKs may help elucidate these effects". The authors pointed out the technical difficulty of obtained sufficient numbers of MK for such analysis, which I accept, and instead analyzed mature platelets, finding no difference between control and DKO platelets. This is not necessarily surprising, since mature circulating platelets have no need to engage an ECM microenvironment, and for the same reason I would suggest that mature platelet analyses are not representative of MK behavior as regards ECM interactions.

https://doi.org/10.7554/eLife.104963.2.sa2

Reviewer #2 (Public review):

Summary:

This study makes a significant contribution to understanding the microenvironment of megakaryocytes (MKs) in the bone marrow, identifying an extracellular matrix (ECM) cage structure that influences MK localization and maturation. The authors provide compelling evidence for the presence of this ECM cage and its role in MK homeostasis, employing an array of sophisticated imaging techniques and molecular analyses.

The authors have addressed most of the concerns raised in the previous review, providing clarifications and additional data that strengthen their conclusions

More broadly, this work adds to a growing recognition of the ECM as an active participant in haematopoietic cell regulation in the bone marrow microenvironment. This work could pave the way to future studies investigating how the megakaryocytes' ECM cage affects their function as part of the haematopoietic stem cell niche, and by extension, influences global haematopoiesis.

https://doi.org/10.7554/eLife.104963.2.sa1

Author response:

The following is the authors' response to the original reviews.

> ***Reviewer #1 (Public review)***
>
> *(1) The authors postulate a synergistic role for Itgb1 and Itgb3 in the intravasation phenotype, because the single KOs did not replicate the phenotype of the DKO. However, this is not a correct interpretation in the opinion of this reviewer. The roles appear rather to be redundant. Synergistic roles would rather demonstrate a modest effect in the single KO with potentiation in the DKO.*

We agree that the interaction between Itgb1 and Itgb3 appears redundant and we have corrected this point in the revised manuscript (page 10).

> *(2) The experiment does not explain how these integrins influence the interaction of the MK with their microenvironment. It is not surprising that attachment will be impacted by the presence or absence of integrins. However, it is unclear how activation of integrins allows the MK to become "architects for their ECM microenvironment" as the authors posit. A transcriptomic analysis of control and DKO MKs may help elucidate these effects.*

We do not yet understand how the activation of α5β1 or αvβ3 integrins affects ECM remodeling by megakaryocytes. Integrins are key regulators of ECM remodeling (see https://doi.org/10.1016/j.ceb.2006.08.009) and can transmit traction forces that induce these changes (see https://doi.org/10.1016/j.bpj.2008.10.009). Our previous study also found reduced RhoA activation in double knockout (DKO) megakaryocytes (MKs) (Guinard et al., 2023, PMID: 37171626), which likely affects ECM organization. These findings are discussed in the Discussion section of the paper (page 14).

As suggested, conducting a transcriptomic analysis of control and DKO MKs may help to elucidate these effects. However, isolating native rare MKs from DKO mice is technically challenging and requires too many animals. To overcome this issue, we instead isolated mouse platelets and used targeted RT-PCR arrays to profile key ECM remodelling (ECM proteins, proteases…) and adhesion molecules (Zifkos et al., Circ. Res. 2024, PMID, 38563147). Quality controls confirmed that integrin RNA was undetectable in the DKO samples, ruling out contamination. Nevertheless, we found no significant expression differences exceeding the 3-fold change threshold between the control and DKO groups. The high Ct (threshold cycles) values indicate low transcript abundance, which may mask subtle changes (see the scatter plot below). As an example, we present a typical result obtained for the reviewer.

Author response image 1.

Relative expression comparison of ECM related-genes between control and DKO integrins in washed platelets. The figure shows a log transformation plot of the relative expression level of each gene between normal (x-axis) and DKO integrins (y-axis). The lines indicate the threefold change threshold for gene expression. These are representative results from two independent experiments.

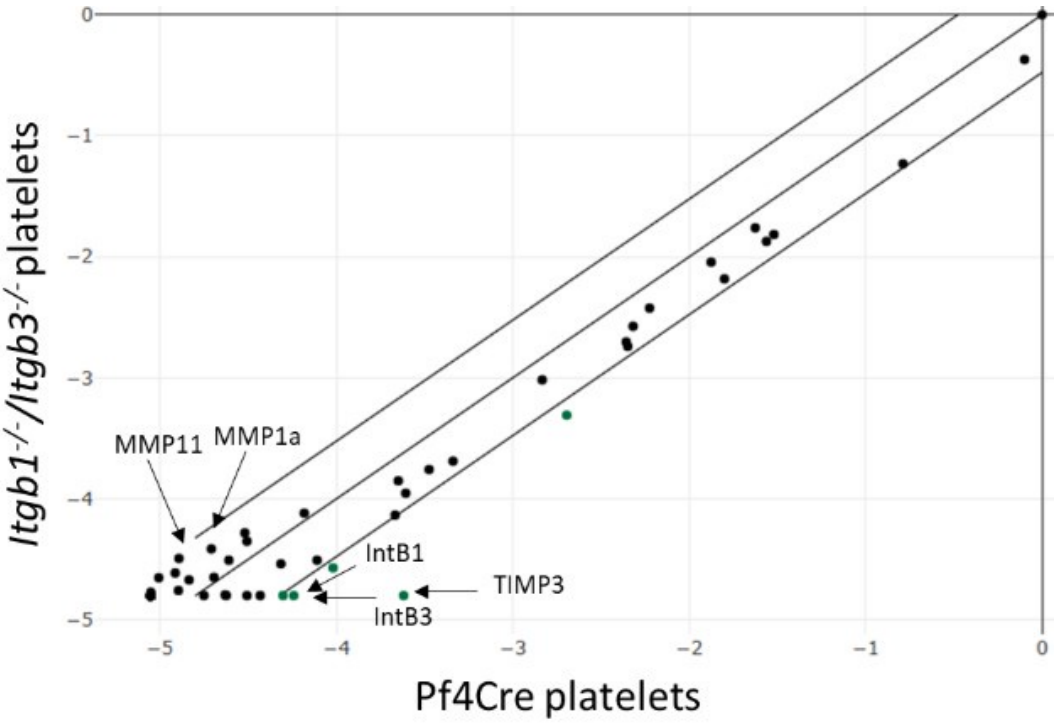

> *(3) Integrin DKO have a 50% reduction in platelets counts as reported previously, however laminin α4 deficiency only leads to 20% reduction in counts. This suggests a more nuanced and subtle role of the ECM in platelet growth. To this end, functional assays of the platelets in the KO and wildtype mice may provide more information.*

The exact contribution of the extracellular matrix (ECM) cage to platelet growth remains incompletely understood. In the Lamα4$^{-/-}$ model, a collagen-rich ECM cage persists alongside normal fibronectin deposition. By contrast, the integrin DKO model exhibits a markedly severe phenotype characterized by the loss of both the laminin cage and collagen and the absence of fibrillar fibronectin. Also, the preserved collagen and fibronectin in Lamα4$^{-/-}$ mice may permit residual activation of signaling pathways - potentially via integrins or alternative mechanisms- compared to the DKO model. We appreciate the reviewer's feedback on this adjustment, which has been incorporated into the discussion (page 15).

As suggested by the reviewer, we performed functional assays that demonstrated normal platelet function in Lamα4$^{-/-}$ mice and impaired integrin-mediated aggregation in Itgb1$^{-/-}$/Itgb3$^{-/-}$ mice, as shown by the new data presented in the publication (see pages 7 and 9). Platelet function remained preserved following treatment with MMP inhibitors. This supports the idea that differences in ECM composition can influence the signaling environment and megakaryocyte maturation, but do not fully abrogate platelet function (page 15).

> *(4) There is insufficient information in the Methods Section to understand the BM isolation approach. Did the authors flush the bone marrow and then image residual bone, or the extruded bone marrow itself as described in PMID: 29104956?*

Additional methodological information has been provided to clarify that only the extruded bone marrow, and not the bone itself, is isolated (page 17).

> *(5) The references in the Methods section were very frustrating. The authors reference Eckly et al 2020 (PMID : 32702204) which provides no more detail but references a previous publication (PMID: 24152908), which also offers no information and references a further paper (PMID: 22008103), which, as far as this reviewer can tell, did not describe the methodology of in situ bone marrow imaging.*

To address this confusion, we have added the reference "In Situ Exploration of the Major Steps of Megakaryopoiesis Using Transmission Electron Microscopy" by C. Scandola et al. (PMID : 34570102) in the « Isolation and preservation of murine bone marrow » section (page 20), which provides a standardized protocol for bone marrow isolation and in situ bone marrow imaging.

> *Therefore, this reviewer cannot tell how the preparation was performed and, importantly, how can we be sure that the microarchitecture of the tissue did not get distorted in the process?*

Thank you for pointing this out. While we cannot completely rule out the possibility of distortion, we have clarified the precautions taken to minimize it. We used a double fixation procedure immediately after bone marrow extrusion, followed by embedding it in agarose to preserve its integrity as much as possible. We have elaborated on this point in greater detail in the Methods section of the revised version (page 18).

> ***Reviewer #2 (Public review):***
>
> *(1) ECM cage imaging*
>
> *(a) The value or additional information provided by the staining on nano-sections (A) is not clear, especially considering that the thick vibratome sections already display the entirety of the laminin γ1 cage structure effectively. Further clarification on the unique insights gained from each approach would help justify its inclusion.*

Ultrathin cryosectioning enables high-resolution imaging with a threefold increase in Z-resolution, facilitating precise analysis of signal superposition. This approach was particularly valuable for clearly visualizing activated integrin in contact with laminin and collagen IV fibers (see Fig. 3 in revised manuscript, pages 6, 8 and 18). Additionally, 3D reconstructions and z-stack data reveal complex interactions between the basement membrane and the cellular ECM cage that are not evident in 2D projections (see page 6). These complementary methods help elucidate the detailed molecular and three-dimensional organization of the ECM cage surrounding megakaryocytes. These points have been clarified in the method and result sections.

> *(b) The sMK shown in Supplementary Figure 1C appears to be linked to two sinusoids, releasing proplatelets to the more distant vessels. Is this observation representative, and if so, can further discussion be provided?*

This observation is not representative; MKs can also be associated with just one sinusoid.

> *(c) Freshly isolated BM-derived MKs are reported to maintain their laminin γ1 cage. Are the proportions of MKs with/without cages consistent with those observed in microscopy?*

After mechanical dissociation and size exclusion, almost half of the MKs successfully retained their cages (53.4% ± 5.6%, based on 329 MKs from three experiments; see page 7 of the manuscript for new data). This highlights the strong physical connection between MK and their cage.

> *(2) ECM cage formation*
>
> *(a) The statement "the full assembly of the 3D ECM cage required megakaryocyte interaction with the sinusoidal basement membrane" on page 7 is too strong given the data presented at this stage of the study. Supplemental Figure 1C shows that approximately 10% of pMKs form cages without direct vessel contact, indicating that other factors may also play a role in cage formation.*

The reviewer is correct. We have adjust the text to reflect a more cautious interpretation of our results. « Althought we cannot exclude that ECM cage can be form on its own, our data suggests that ECM cage assembly may require interactions between megakaryocytes and the sinusoidal basement membrane » suggests that the assembly of the 3D ECM cage may require interactions between megakaryocytes and the sinusoidal basement membrane » (page 7).

> *(b) The data supporting the statement that "pMK represent a small fraction of the total MK population" (cell number or density) could be shown to help contextualize the 10% of them with a cage.*

Following the reviewer's recommendation, a new bar graph has been added to illustrate the 18 ± 1.3 % of MK in the parenchyma relative to the total MK in the bone marrow (page 7 and Suppl. Figure 1H).

> *(c) How "the full assembly of the 3D ECM cage" is defined at this stage of the study should be clarified, specifically regarding the ECM components and structural features that characterize its completion.*

We recognize that the term ' full assembly' of the 3D ECM cage can be misleading, as it might suggest different stages of cage formation, such as a completed cage, one in the formation process, or an incomplete cage. Since we have not yet studied this concept, we have eliminate the term "full assembly" from the manuscript to avoid confusion. Instead, we mention the presence of a cage.

> *(3) Data on MK Circulation and Cage Integrity: Does the cage require full component integrity to prevent MK release in circulation? Are circulating MKs found in Lama4-/- mice? Is the intravasation affected in these mice? Are the ~50% sinusoid associated MK functional?*

In lamα4-deficient (Lamα4-/-) mice, which possess an intact collagen IV cage but a structurally compromised laminin cage, electron microscopy and whole-mount imaging revealed an absence of intact megakaryocytes within the sinusoidal lumen. This observation indicates that the structural integrity of all components of the ECM cage is critical for preventing megakaryocyte entry into the circulation. Despite the laminin deficiency, mature Lamα4-/- megakaryocytes exhibited normal ultrastructure and maintained typical intravasation behavior. Furthermore, analysis of bone marrow explants from Lamα4-/- mice demonstrated that megakaryocytes retained their capacity to extend proplatelets. These findings are presented on page 7 and further discussed on page 14.

> *(4) Methodology*
>
> *(a) Details on fixation time are not provided, which is critical as it can impact antibody binding and staining. Including this information would improve reproducibility and feasibility for other researchers.*

We have included this information in the methods section.

> *(b) The description of 'random length measuring' is unclear, and the rationale behind choosing random quantification should be explained. Additionally, in the shown image, it appears that only the branching ends were measured, which makes it difficult to discern the randomness in the measurements.*

The random length measurement method uses random sampling to provide unbiased data on laminin/collagen fibers in a 3D cage. Contrary to what the initial image might have suggested, measurements go beyond just the branching ends ; they include intervals between various branching points throughout the cage. This is now explained page 19.

To clarify this process, we will outline these steps page 19 as : 1) acquire 3D images, 2) project onto 2D planar sections, 3) select random intersection points for measurement, 4) measure intervals using ImageJ software, and 5) repeat the process for a representative dataset. This will better illustrate the randomness of our measurements.

> *(5) Figures*
>
> *(a) Overall, the figures and their corresponding legends would benefit from greater clarity if some panels were split, such as separating images from graph quantifications.*

Following the reviewer's suggestion, we will fully update all the Figures and separate images from graph quantifications.

> ***Reviewer #3 (Public review):***
>
> *(1) The data linking ECM cage formation to MK maturation raises several interesting questions. As the authors mention, MKs have been suggested to mature rapidly at the sinusoids, and both integrin KO and laminin KO MKs appear mislocalized away from the sinusoids. Additionally, average MK distances from the sinusoid may also help separate whether the maturation defects could be in part due to impaired migration towards CXCL12 at the sinusoid. Presumably, MKs could appear mislocalized away from the sinusoid given the data presented suggesting they leaving the BM and entering circulation. Additional data or commentary on intrinsic (ex-vivo) MK maturation phenotypes may help strengthen the author's conclusions and shed light on whether an essential function of the ECM cage is integrin activation at the sinusoid.*

The idea that megakaryocytes move toward CXCL12 is still debated. Some studies suggest mature MKs are mainly sessile (PMID: 28743899), while others propose that CXCL12 may guide MK progenitors rather than mature MKs (PMID: 38987596, this reference has been added). To address the reviewer's concerns regarding CXCL12-mediated migration, we conducted additional investigations.

For DKO integrins, Guinard et al. (2023, PMID: 37171626) reported no significant change in the distance between MKs and sinusoids, indicating that integrin deficiency does not impair MK migration toward sinusoidal vessels.

In our own study involving Lamα4-/- mice, we utilized whole-mount bone marrow preparations, labeling MKs with GPIbβ antibodies and sinusoids with FABP4 antibodies. We observed a 1.6-fold increase in the proximity of MKs to sinusoids in Lamα4-/- mice compared to controls (see figure below). However, the absolute distances measured were less than 3 µm in both groups, much smaller than the average diameter of a mature MK (20 - 25 µm), raising questions about the biological significance of these findings in active MK migration. What happens with MK progenitors - a population not detectable in our experiments using morphological criteria or GPIb staining - remains an open question.

These results are provided for the reviewer's information and will be available to eLife readers, along with the authors' responses, in the revised manuscript.

Author response image 2.

Quantification of distance between MK and sinusoids in WT and Lama4$^{-/-}$ mice (in µm, n=3 independent experiments, *P=0.0312 Mann-Whitney test).

Distance:

WT: 1.7 ± 3.8 µm

Lama4$^{-/-}$: 2.7 ± 4.7 µm

Proportion of vessel-associated MK related to total MK (distance MK/sinusoid = 0 µm)

WT: 75% (total MK counted 141)

Lama4$^{-/-}$: 59 % (total MK counted 197)

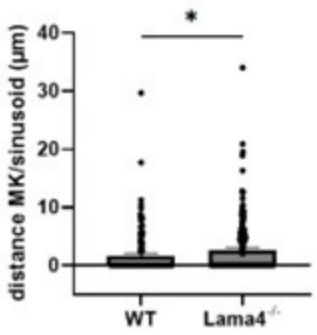

> *(2) The data demonstrating intact MKs in the circulation is intriguing - can the authors comment or provide evidence as to whether MKs are detectable in blood? A quantitative metric may strengthen these observations.*

To investigate this, we conducted flow cytometry experiments and prepared blood smears to determine the presence of intact Itgb1-/-/Itgb3-/- megakaryocytes in the blood. Unfortunately, we could not detect any intact megakaryocytes in the blood samples using FACS (see new Supplementary Figure 4E) nor any on the blood smears (data not shown). However, we observed that large, denuded megakaryocyte nuclei were retained in the downstream pulmonary capillaries of these mice. Intravital imaging of the lung has previously provided direct evidence for the phenomenon of microvascular trapping (Lefrançois et al., 2017; PMID: 28329764), demonstrating that megakaryocytes can be physically entrapped within the pulmonary circulation due to size exclusion while releasing platelets. This has been clarified in the revised paper (Results section, page 10).

> *(3) Supplementary Figure 6 - shows no effect on in vitro MK maturation and proplt, or MK area - But Figures 6B/6C demonstrate an increase in total MK number in MMP-inhibitor treated mice compared to control. Some additional clarification in the text may substantiate the author's conclusions as to either the source of the MMPs or the in vitro environment not fully reflecting the complex and dynamic niche of the BM ECM in vivo.*

This is a valid point. We have revised the text to be more cautious and to provide further clarification on these points (page 12).

> *(4) Similarly, one function of the ECM discussed relates to MK maturation but in the B1/3 integrin KO mice, the presence of the ECM cage is reduced but there appears to be no significant impact upon maturation (Supplementary Figure 4). By contrast, MMP inhibition in vivo (but not in vitro) reduces MK maturation. These data could be better clarified in the text, or by the addition of experiments addressing whether the composition and quantity of ECM cage components directly inhibit maturation versus whether effects of MMP-inhibitors perhaps lead to over-activation of the integrins (as with the B4galt KO in the discussion) are responsible for the differences in maturation.*

We thank the reviewer for pointing this out.

In our study of DKO integrin mice with a reduced extracellular matrix (ECM) cage, we observed normal proportions of MK maturation stages. However, these mutant MKs had a disorganized membrane system and smaller cytoplasmic areas compared to wild-type cells, indicating issues in their maturation. This is detailed further in the manuscript (see page 9).

In the context of MMP inhibition in vivo, which also leads to reduced MK maturation, our immunofluorescence analysis revealed in an increased presence of activated β1 integrin in bone marrow sections (see Supplementary Figure 6E). As suggested by the reviewer, this increase may explain the maturation defect.

In summary, while it's challenging to definitively determine how ECM cage composition and quantity affect MK maturation in vivo, our results show that changes to the ECM cage - whether through genetic modification (DKO) or MMP inhibition - are consistently linked to defects in MK maturation.

> ***Reviewer #1 (Recommendations for the authors):***
>
> *(1) Movies 1-3 are referenced in the Results section, but this reviewer was not able to find a movie file.*

They have now been added to the downloaded revised manuscript.

> *(2) Figure 2D is referenced in the Results Section but this panel is not present in the Figure itself. Instead, this seems to be what is referred to as the right panel of 2C.*

Thank you. Following the suggestion of reviewer 2, we have now split the panels and separated the images from the graph quantifications. This change has modified all the panel annotations, which we have carefully checked both in the legend and in the manuscript.

> *(3) Supplemental Fig 3C has Fibrinogen quantification which seems to belong in Supplemental 3 F instead.*

Supplementary Figure 3C serves as a control for immunofluorescence, indicating that no fibrinogen-positive granules are detectable in the DKO mice. This supports the conclusion that the αIIbβ3 integrin-mediated fibrinogen internalization pathway is non-functional in this model, affirming the bar graph's placement. We appreciate the reviewer's insight that similar results may arise from the IEM experiments in Figure 3H, which is valuable for strengthening our findings.

> *(4) The x-axis labels in Supplemental 5B are not uniform.*

This has be done. Thank you.

> ***Reviewer #2 (Recommendations for the authors):***
>
> *(1) Figure 1 Panel C: The sinusoidal basement membrane staining is missing, making it difficult to conclude that the collagen IV organization extends radially from the sinusoidal basement membrane.*

As recommended by the reviewer, we have updated Figure 1C with a new image illustrating the basement membrane (FABP4 staining) and the collagen IV cage. This new image confirms that the cage extends radially from the basement membrane.

> *(2) Arrows in 1B: Based on the arrow's localisation, the description of "basement membrane-cage connection" is not evident from the images as it looks like the signal*

> *colocalization (right lower panel) occurs below the highlighted areas. Clarification or additional evidence of co-localization is required.*

The apparent localization of the signal "below" the highlighted areas in the maximal projection image is due to the nature of 2D projections, which compress overlapping signals from multiple depths within the bone marrow into a single plane. This can obscure the spatial relationship between the basement membrane and extracellular matrix (ECM) components. However, when the complete z-stack series is examined, the direct connection between the basement membrane and the ECM cage becomes evident in three dimensions. Therefore, we have now added a comprehensive analysis of the entire z-stack dataset, allowing us to accurately interpret the spatial relationships between the basement membrane and ECM in the native bone marrow microenvironments (movies 1 and 2, and Suppl. Figure 1D-E).

> *(3) In Figure 4C, GPIX is used to identify MKs by IVM while GP1bβ is used throughout the rest of the manuscript. It would be helpful for readers who are less familiar with MKs to understand whether GPIX and GP1bβ identify the same population of MKs and the rationale for choosing one marker over the other.*

GPIX and GPIbβ are components of the GPIb-IX complex, identifying mature megakaryocytes (Lepage et al., 2000, PMID : 11110688). The choice of one over the other in different experiments is primarily based on technical considerations. The intravital experiments have been standardized using an AF488-conjugated anti-GPIX to identify mature megakaryocytes consistently. GPIbβ (GP1bβ) is used in the rest of the manuscript due to its strong and specific bright staining. We have clarified this point in the Result (page 10) and in the Material/methods section (page 17).

> *(4) The term "total number of MKs" is used (p8), but the associated data presented in the figure reflect MK density per surface area. Descriptions in the text should align with the data format in the figures.*

This has been corrected in the revised manuscript (page 8). Thank you.

> *(5) Supplemental Figure 1(B): Collagen I is written as Collagen III in the legend.*

This has been corrected in the legend of the Figure 1B.

> *(6) Figure 2D is described in the text but is missing from the figure.*

This has been corrected.

> *(7) Supplemental Figure 3: Plot E overlaps with the images, making it unclear.*

To minimise overlap with the images, we've moved the graph with the bars down. Thank you.

> *(8) Supplemental Figure 7: The image quality is too low, and spelling underlining issues are present. A better-quality version with clear labelling is essential.*

We have improved the quality of Figure 7 and fixed the underlining problems.

> *(9) The movies were not found in the downloads provided.*

They have now been added to the downloaded revised manuscript.

> *(10) Some bar graphs are missing the individual data points.*

All figures have been standardized and now include the individual data points.

> ***Reviewer #3 (Recommendations for the authors):***
>
> *Some minor comments:*
>
> *(1) If there is specific importance to some of the analyses of the cage structure, such as fiber length, and pore size, (eg. if they may have biological significance to the MK) it may help readers to give additional context to what differences in the pore size might imply. For example, do pores constrain MKs at sites where actin-driven proplatelet formation could be initiated?*

The effects of extracellular matrix (ECM) features - like fiber length and pore size - on megakaryocyte (MK) biology are not fully understood. Longer ECM fibers may help MKs adhere better and sense their environment. Larger pores could make it easier for MKs to grow, communicate, and extend proplatelets through blood vessel walls. The role of matrix metalloproteinases (MMPs), which degrade the ECM, adds to the complexity, and how this occurs in vivo is not yet well understood.

As suggested, some of these points have been addressed in the revised manuscript (Discussion, page 16).

> *(2) "Although fibronectin and fibrinogen were readily detected around megakaryocytes, a reticular network around megakaryocytes was not observed. Furthermore, no connection was identified between fibronectin and fibrinogen deposition with the sinusoid basement membrane, in contrast to the findings for laminin and collagen IV (Supp. Figures 1E)." - Clarification of how these data are interpreted might be helpful as to what the authors are intending to demonstrate with these data as at least in Figure 1E, fibronectin, and fibrinogen do appear expressed along the MK surface and at the sinusoidal-MK interface.*

While fibronectin and fibrinogen are present around megakaryocytes and at the vessel-cell interface, they do not form a reticular ECM cage. The functional implications of this finding remain unclear. One can imagine that the specific spatial arrangement of various ECM components may lead to different functional roles. Laminin and collagen IV may provide structural support by forming a 3D cage that is essential for the proper positioning and maturation of megakaryocytes. In contrast, fibronectin and fibrinogen may have different functions, potentially related to megakaryocyte expansion in bone marrow fibrosis (Malara et al., 2019, PMID : 30733282) and (Matsuura et al., 2020, PMID : 32294178).

This topic has been adressed in the Results page 7 and discussion on page 13.

> *(3) Given the effects of dual B1/B3 integrin inhibition on MK intravasation, can the authors comment on the use of integrin RGD-based inhibitors? Are these compounds and drugs likely to interfere with MK retention?*

Our study shows that MK retention depends on the integrity of both components of the cage, collagen IV and laminin (see also point 3 of reviewer 2). Collagen IV contains RGD sequences, making it susceptible to RGD-based inhibition, whereas laminin does not utilize the RGD motif, raising questions about the overall efficacy of these inhibitors.

In addition, the in vivo efficacy and potential off-target effects of these inhibitors in the complex bone marrow microenvironment remain to be fully elucidated. This intriguing issue

warrants further investigation.

> *(4) Beyond protein components, other non-protein ECM molecules including glycosaminoglycans (HA, HS) have essential roles in supporting MK function, including maturation (PMIDs: 31436532, 36066492, 27398974) and may merit some brief discussion if the authors feel this is helpful.*

We followed reviewer's suggestion and mention the contribution of glycoaminoglycans in MK maturation. We also added the three references (page 13).

> *(5) In several locations, the text refers to figure panels that are either not present or not annotated correctly (some examples include Figure 2D, Supplementary Figure 3E vs 3D).*

Following the suggestion of reviewer 2, we have now split the panels and separated the images from the graph quantifications. This change has changed all the panel annotations, which we have carefully checked both in the legend and in the manuscript.

> *(6) In some cases, the figure legends seem to incorrectly refer to text, colors, or elements in the panels (e.g. Supplementary Figure 3, fibrinogen is referred to as yellow in the legend but is green in the figure). In Supplemental Figure 1, an image is annotated as pryenocyte in the figure, but splenocyte in the text.*

This has been corrected in the figures and in the revised manuscript. Please also see point (7) below. Thank you very much.

> *(7) Images demonstrating GPIX and GPIBb positive cells in the calvarial and lung microcirculation are convincing, but in Figure C these cells are referred to as MKs, whereas in Figure D they are referred to as pyrenocytes (as well as in the discussion). It is not clear if this is intentional and refers to bare nuclei from erythrocytes or indeed refers to MKs or MK nuclei. Clarification would help guide readers.*

We agree with the reviewer and fully acknowledge the need for clarification. We confirm that these circulating cells are megakaryocytes. To avoid confusion, we have ensure that all references to "pyrenocytes" have been replaced with "megakaryocytes."

https://doi.org/10.7554/eLife.104963.2.sa0